

AD-A129 699

BRUSHLESS SUPERCONDUCTING GENERATOR(U) CASE WESTERN
RESERVE UNIV CLEVELAND OHIO DEPT OF ELECTRICAL
ENGINEERING AND APPLIED PHYSICS O K MAWARDI ET AL.

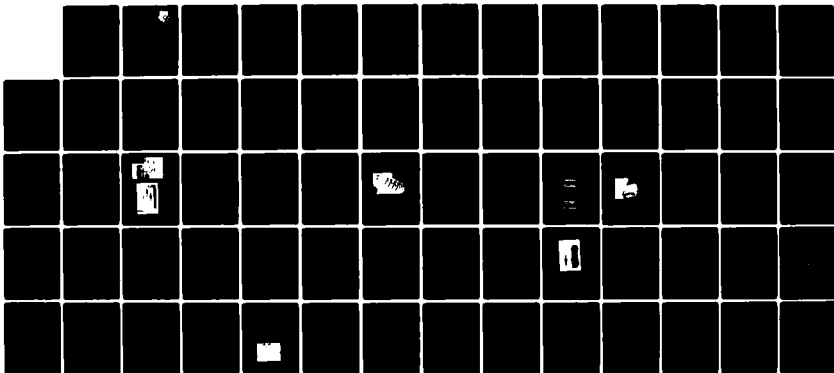
1/1

UNCLASSIFIED

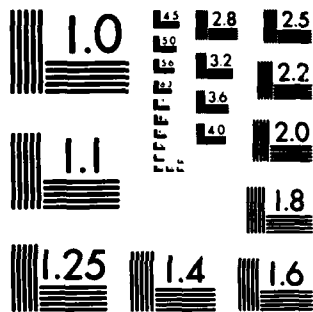
OCT 82 AFWAL-TR-82-2097 F33615-79-C-2038

F/G 10/2

NL



END
DATE
FILMED
7 83
DTIC



MICROCOPY RESOLUTION TEST CHART
NATIONAL BUREAU OF STANDARDS-1963-A

AFWAL-TR-82-2097

BRUSHLESS SUPERCONDUCTING GENERATOR



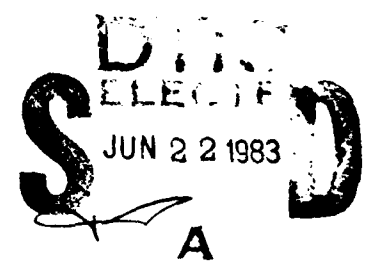
CASE WESTERN RESERVE UNIVERSITY
UNIVERSITY CIRCLE
CLEVELAND, OHIO 44106

OCTOBER 1982

FINAL REPORT FOR PERIOD APRIL 1979 - JUNE 1982

Approved for public release; distribution unlimited

AERO PROPULSION LABORATORY
AIR FORCE WRIGHT AERONAUTICAL LABORATORIES
AIR FORCE SYSTEMS COMMAND
WRIGHT-PATTERSON AIR FORCE BASE, OHIO 45433



ADA 1 29699

DTIC FILE COPY

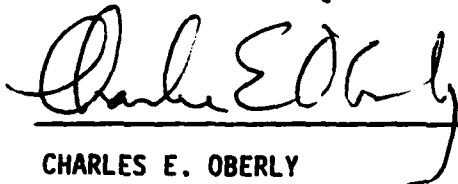
83 06 20 05 6

NOTICE


When Government drawings, specifications, or other data are used for any purpose other than in connection with a definitely related Government procurement operation, the United States Government thereby incurs no responsibility nor any obligation whatsoever; and the fact that the government may have formulated, furnished, or in any way supplied the said drawings, specifications, or other data, is not to be regarded by implication or otherwise as in any manner licensing the holder or any other person or corporation, or conveying any rights or permission to manufacture use, or sell any patented invention that may in any way be related thereto.

This report has been reviewed by the Office of Public Affairs (ASD/PA) and is releasable to the National Technical Information Service (NTIS). At NTIS, it will be available to the general public, including foreign nations.

This technical report has been reviewed and is approved for publication.



CHARLES E. OBERLY
Project Engineer
Power Systems Branch



WILLIAM U. BORGER
Technical Area Manager
Power Systems Branch
Aerospace Power Division

FOR THE COMMANDER



JAMES D. REAMS
Chief, Aerospace Power Division
Aero Propulsion Laboratory

"If your address has changed, if you wish to be removed from our mailing list, or if the addressee is no longer employed by your organization please notify AFNAL/POOS, W-PAFB, OH 45433 to help us maintain a current mailing list".

Copies of this report should not be returned unless return is required by security considerations, contractual obligations, or notice on a specific document.

Unclassified

SECURITY CLASSIFICATION OF THIS PAGE (When Data Entered)

REPORT DOCUMENTATION PAGE		READ INSTRUCTIONS BEFORE COMPLETING FORM
1. REPORT NUMBER AFWAL-TR-82-2097	2. GOVT ACCESSION NO. AD-A129699	3. RECIPIENT'S CATALOG NUMBER
4. TITLE (and Subtitle) BRUSHLESS SUPERCONDUCTING GENERATOR		5. TYPE OF REPORT & PERIOD COVERED Final Report for Period Apr 79 - Jun 82
		6. PERFORMING ORG. REPORT NUMBER
7. AUTHOR(s) O. K. Mawardi and Altan M. Ferendeci		8. CONTRACT OR GRANT NUMBER(s) F33615-79-C-2038
9. PERFORMING ORGANIZATION NAME AND ADDRESS Department of Electrical Engineering Case Western Reserve University University Circle, Cleveland, Ohio 44106		10. PROGRAM ELEMENT, PROJECT, TASK AREA & WORK UNIT NUMBERS 31453251
11. CONTROLLING OFFICE NAME AND ADDRESS Aero Propulsion Laboratory (AFWAL/POOS) Air Force Wright Aeronautical Laboratories (AFSC) Wright Patterson Air Force Base, Ohio 45433		12. REPORT DATE October 1982
		13. NUMBER OF PAGES 62
14. MONITORING AGENCY NAME & ADDRESS (if different from Controlling Office)		15. SECURITY CLASS. (of this report) Unclassified
		15a. DECLASSIFICATION, DOWNGRADING SCHEDULE
16. DISTRIBUTION STATEMENT (of this Report) Approved for public release; distribution unlimited		
17. DISTRIBUTION STATEMENT (of the abstract entered in Block 20, if different from Report)		
18. SUPPLEMENTARY NOTES		
19. KEY WORDS (Continue on reverse side if necessary and identify by block number) Flux Pump Superconducting Alternator Brushless Generator		
20. ABSTRACT (Continue on reverse side if necessary and identify by block number) This report covers work on a flux pump excited brushless brushless superconducting alternator. The flux pump, used to provide the excitation current of the field coils incorporates several features of a machine studied theoretically and reported in an earlier paper. The flux pumping is achieved with six electromagnets having pole pieces of special configurations to yield high efficiency and rapid pumping rates. The maximum design values for the current in the pump is 1,300 amps and for the rotational speed, 500 rpm. Sensors installed on the generator yield information		

DD FORM 1473
1 JAN 73

UNCLASSIFIED

SECURITY CLASSIFICATION OF THIS PAGE (When Data Entered)

Unclassified

SECURITY CLASSIFICATION OF THIS PAGE(When Data Entered)

→ on the spatial and temporal behavior of the magnetic field in the flux spot and on the operational characteristics of the pump. The preliminary observations are compared with theoretical predictions. ↖

Unclassified

SECURITY CLASSIFICATION OF THIS PAGE(When Data Entered)

FOREWORD

The applied superconductivity team in the Department of Electrical Engineering and Applied Physics of Case Western Reserve University has been active for several years in developing an understanding of the rotating spot flux pump.

This report summarizes the many years' effort of this group and describes the incorporation of this device in a superconducting rotating machine.

The authors wish to express their appreciation to many colleagues who have contributed helpful ideas and suggestions. In particular, they wish to thank H. Laquer, S. Wipf, W. Hassenzahl and C. Oberley. They are also indebted to J. Parker for the loan of the instrumentation slip rings.



Accession by	
NTIS Class	<input checked="" type="checkbox"/>
DTIC TAB	<input type="checkbox"/>
Unannounced	<input type="checkbox"/>
Justification	
By	
Prescription/	
Availability Codes	
Dist	Special
A	

TABLE OF CONTENTS

SECTION	PAGE
I INTRODUCTION	1
II CHARACTERISTICS OF FLUX PUMP	5
1. Fundamental Features of Flux Pump	5
2. Design Parameters of the Flux Pump	9
III CONSTRUCTION FEATURES OF GENERATOR	18
1. Rotor-Dewar	18
2. Field-(Excitation) Coils	22
3. Flux Pump	26
IV CASING AND STATOR	30
1. Armature Coils	32
2. Flux-Pump Magnets	32
3. Vacuum System	36
V INSTRUMENTATION	39
1. Stator	39
2. Rotor	39
VI ASSEMBLY OF GENERATOR	42
VII COOLING AND OPERATION	44
VIII MEASUREMENTS AND RESULTS	44
1. Static Measurements	44
2. Dynamic Measurements	46
a. Histogram of Field-coils Current	49
b. Behavior of Induced Voltage	51
3. Energy Losses in the Flux Pump	52
4. Maximum Pump Current	53
IX SCALING LAWS FOR FLUX PUMPS	55
X CONCLUSION	56
REFERENCES	58
BIBLIOGRAPHY	59
XI HAZARD ANALYSIS	62

PREVIOUS PAGE BLANK-NOT FILLED

LIST OF ILLUSTRATIONS

FIGURE		PAGE
1	Idealized Drawing For Brushless Superconducting Generator Discussed in Ref. (1).	2
2	Schematic of Rotating Spot Flux Pump	6
3	Idealized pump of Volger's Design (Ref. 3)	6
4(a)	Frame of Reference Used In The Calculations	12
4(b)	Distribution of the y-component of the Magnetic Field In The Normal Spot	12
4(c)	Configuration of the Eddy Current Circulating in the Normal Spot	12
5	Accurate Distribution of Magnetic Field in Leading Edge of Boundary Layer of Spot (Ref. 8)	15
6	Dependence of the Effective Inductance L_{eff} and Resistance R_{eff} of the Normal Spot as a Function of the Reynolds number R_m .	15
7	Equivalent Circuit Diagram for Flux Pump	17
8	Engineering Details for Superconducting Brushless Generator	19
8(a)	General View of Generator, Together with the Vacuum and Cryogenic systems	20
8(b)	Photograph of Vacuum Vessel	20
9	General Layout for Superconducting Field Coils	23
9(a)	Photograph of Field Coils Mounted on Former	24
10	Schematic Diagram for Flux Pump	27
10(a)	Photograph of Nitrogen Cooled Electromagnets for Flux Pump	28
11	Magnetization Curves for Electromagnets Used In the Excitation of the Flux Pump	37
12	Magnetic Field in the Air Gap of the Flux Pump for Different Excitations of the Electromagnet.	38
13	Schematic for the Location of the Sensing Devices Referred to in the Text	40
13(a)	Photograph of Flux Pump and Field Windings Showing Location of, and Connections to the Sensors	41

LIST OF ILLUSTRATIONS, CON'T

FIGURE		PAGE
14	D.C. Current Transformer Used to Measure the Flux Pump Current	43
15	Dynamic Measurement of the No-load Magnetic Field in the Air Gap of the Flux Pump	45
16	First Trial Histogram for the Build-up of the Current in the Field Coils	47
17	Typical Histogram Demonstrating the Ability of the Pump, to Go Through the Various Modes of Operation as expected	48
18	Dependence of the Rate of Charging on the Speed of Rotation	50
19	Temporal Dependence of the Voltage Induced Across the Superconducting Belt	50
20	Dependence of the Normalized Maximum Current Generated by the Pump as a Function of the speed of Rotation (or Reynolds number R_m)	54

SUMMARY

This report describes a theoretical and experimental investigation to demonstrate the feasibility of a brushless superconducting electric generator. The main feature of the concept is to use a flux pump to excite the superconducting field windings and effectively convert them into "permanent electromagnets".

The main thrust of the theoretical effort was to predict the characteristics of the flux pump as a current generator and to determine its performance as a function of the speed of rotation, the strength of the field in the air gap of the flux pump and the shape of the magnets.

The report goes in some details in the method of construction of the generator and in the diagnostics used to test the overall performance of the generator.

The results obtained have been very encouraging and conclusively establish the feasibility of the machine. The tests show also that very high overall efficiencies (better than 95%) can be obtained and that fast pumping rates (of the order of milliseconds) are feasible.

SECTION I INTRODUCTION

The concept of a.c. superconducting generators has been of great interest for several years. Already a number of experimental prototypes have been constructed. The state-of-the-art in the engineering of these machines has advanced to the point that a variety of machines with capacities as high as 300 MVA have been designed.

In all of these generators, the field windings are constructed out of superconducting material and are rotated. The armature is placed outside the field, is wound with normal conductors and is stationary. This arrangement allows for improved cooling of the armature winding and optimizes the use of conductors (product of magnetic flux density and current density).

In most rotating field windings designs the coils are terminated in slip rings. These rings and brushes are necessary to complete the circuit of the field windings and the source of the excitation current. The use of brushes has the disadvantage of introducing thermal losses at the normal-superconducting (N/S) wire junctions. thus requiring greater refrigeration capacity. Now, several long range plans for space missions have considered including superconducting generators in the power system. In order for such plants to be feasible, it is essential to keep weight to a minimum. It is very desirable, therefore, to eliminate, if possible, the thermal losses at the leads i.e. at the N/S junctions.

Another desirable feature of the slip-rings is the electrical noise they generate at the brushes contact points and which can interfere with the air-borne communication equipment.

A novel scheme developed by Mawardi⁽¹⁾, and which has been reported in the literature dispenses completely with the use of slip rings. In this scheme, the field windings are energized by a flux pump of the rotating flux spot type. The field coils and the flux pump form an integral superconducting system that

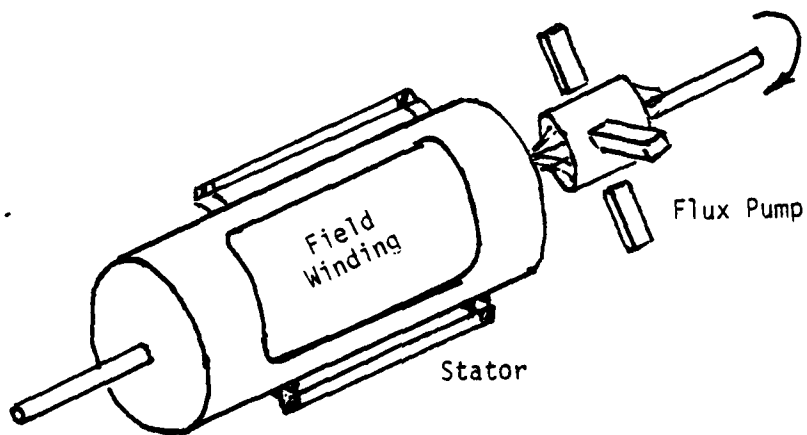


Figure 1 - Idealized Drawing For Brushless Superconducting Generator Discussed In Ref. (1).

bodily rotate together. Once the field windings are charged, they behave as a permanent superconducting electromagnet. (Fig. 1).

To fix the ideas, the potential benefits of a brushless superconducting generator of the type discussed here, will be reviewed. A 20 MW superconducting generator presently being constructed by GE requires a 350 KVA excitation power for its field coils. The generator is a four pole machine with the maximum current in the field coils being 980 amps. In spite of the latest state-of-the-art design of the brushes, a potential drop of 0.2 volts is expected to occur at the brushes. Accordingly, 196 watts are continuously dissipated at the down leads.

The use of a flux pump completely eliminates the refrigeration of the down lead. This refrigeration load is actually equivalent to 500% the thermal losses from the rotor alone. Furthermore, the rotating flux pump which allows the charging of the coils, does not need to remain in operation once the maximum current is attained. As a result, the weight of the flux pump is considerably less than that of the excitation power plant. It is expected, therefore, that the combined weight of the refrigeration and excitation power plants of a brushless machine to be between 1/3 to 1/5 that of a machine with slip rings.

The success in the construction of a brushless generator of the type referred to above will rest on the proper design of the flux pump. For this reason, a major portion of the research effort reported here has been devoted to the development of an efficient flux pump.

The present report is divided in several sections. In the first of these sections, the basis for the operational characteristics of the flux pump is discussed in great details. The subsequent four sections are devoted to a description of the constructional details of the generator, as well as, to the diagnostics used to experimentally verify the performance of the generator.

The report ends with an account of the tests that have been conducted and with a discussion of the interpretation of the experimental results. The conclusions reached are that the brushless superconducting generator is a very promising machine which shares several features of conventional superconducting machines but which, in addition, possesses a very attractive figure of merit expressed in terms of power generated per unit of dead weight. Furthermore, it has a high efficiency and can have a fast charging (and/or discharging) time.

SECTION II

CHARACTERISTICS OF FLUX PUMP

1. Fundamental Features of Flux Pump

The flux pump is a device capable of changing the magnetic flux in a superconducting circuit while preserving the integrity of the electric circuit. Several types of flux pumps have been invented (2). The type selected for the work described in this report is the rotating spot flux pump.

The rotating spot flux pump is shown in schematic form in Figure 2. Actually, it consists of a cylindrical sheet of niobium mounted on a shaft capable of spinning about its axis AA'. Several pairs of magnets (or electromagnets) are arranged in a concentric pattern around the sheet.

The poles of the magnets (or electromagnets) facing the sheet have the same polarity and the field strength they produce at the surface of the sheet is high enough to cause the niobium to quench to the normal state over a small region referred to as the "spot". Conductors are periodically connected to the sheet and are then grouped together at A and A', which constitute the output terminals of the pump.

The theory of operation of the flux pump is quite complicated and it is understood only in broad lines. One of the best explanations is obtained by examining the earliest version of the flux pump as invented by Voiger and Admiraal (3). Their device consists of a thin superconducting disc which is cooled down in the presence of a small permanent magnet (Fig. 3). Because of the magnet, a local region of the disc

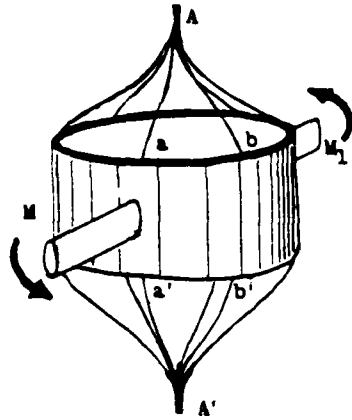


Figure 2 - Schematic Of Rotating Spot Flux Pump. M & M₁ Are Magnets With Poles Of Similar Polarity Facing The Niobium Belt. The Belt Rotates About The Axis AA'. Leads Connected At Equal Intervals a,b,... Collect The Current From The Pump.

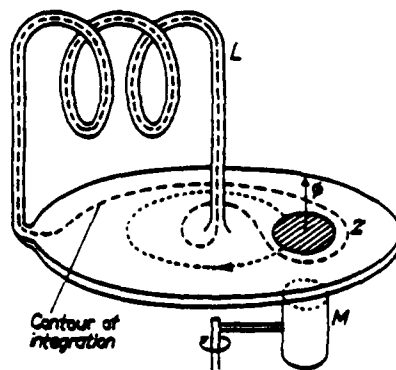


Figure 3 - Idealized Pump Of Volger's Design (Ref. 3) In The Volger's Pump The Magnet M Rotates While The Superconducting Sheet Is Stationary. Z Is The Contour Of Integration Used To Estimate The Flux Linkage To the Load Coil L.

remains normal when the temperature is cooled down below the critical temperature. The magnet is now rotated around the center of the superconducting disc to which a superconducting circuit has been connected as shown in Figure 3.

But it is known that as long as the Meissner effect exists (we exclude for a moment the intermediate state of Type I superconductors, as well as, the mixed state of Type II and Type III superconductors), a simply connected body repels the magnetic field. A doubly connected body such as a ring under the same conditions obeys the laws of conservation of magnetic flux by which it is enclosed. In a triply connected body, an extra degree of freedom appears as discussed below. First, it is important to remember that the topology of the superconducting body is defined by the surface of the superconducting phase rather than the physical surface of the body.

A careful inspection of the current path in the superconducting disc (of Figure 3) in which a region of normal state has been produced leads one to identify the path to be on a triply connected surface. This means that the moving magnetic field lines of the magnet intersect the closed superconducting circuit twice if the magnet was made to go around twice. Indeed, the field lines intersect the disc once where the cluster of moving normal regions is formed and the rest of the superconducting circuit one more time. Similarly, as the magnet is made to go around n times, the field lines intersect the circuit n times. If the flux through the normal region is ϕ_0 , the flux linkage with the superconducting circuit becomes $n\phi_0$. The apparent violation

of the law of conservation of flux is obviously due to the ambiguity in the choice of the integration contour defining the flux to be conserved when a triply connected body is given.

The current circulating in the superconducting circuit is readily evaluated from the relation

$$n\phi_0 = LI \quad (1)$$

where L is the inductance of the circuit and, of course, I is the current.

The moving magnetic field lines of the magnet produce an electromotive force in the normal region and in a part of the superconducting circuit. The electromotive force in the normal region, however, does not give rise to a current through the superconducting circuit: only to eddy currents in the normal region. The induced electromotive force in the superconducting circuit, on the other hand, drives the current defined by Eq. 1. There is a reaction of the current circulating in the superconducting circuit on the flux trapped in the disc. This reaction is reflected in a torque exerted on the permanent magnet producing the moving spot ⁽⁴⁾. The energized coil in the superconducting circuit acts as a spring which is able to reverse the shaft of the superconducting flux pump and convert the magnetic energy into mechanical energy.

To minimize the latter effect, the topology of Figure 2 is used and the permanent magnets are substituted with electromagnets. The performance of flux pumps with this modified configuration has been investigated by a number of workers ⁽⁵⁾ and was shown to be superior to the Volger flux pump.

2. Design Parameters of the Flux Pump

When investigating the performance of a flux pump, the usual notion of voltage and current as used in a conventional electrical machine are valid provided they are derived correctly. Now, the expression of Eq. (1) is not convenient to use in the calculations. Instead, it is more expedient to introduce the average voltage V induced across the belt of superconducting material (potential difference across AA' of Fig. 2). This voltage is given by

$$V = f\phi \quad (2)$$

where ϕ is the flux intersecting the superconducting circuit per cycle and f is the frequency of rotation. The current I (apart from a ripple) produced in the load inductance L is found from

$$L \frac{dI}{dt} = V \quad (3)$$

or

$$I = \frac{V}{L} t = f\phi t \quad (4)$$

It is clear, by comparison of (4) with (1) that $n = ft$.

Usually, the flux pump is actuated by N poles. Consequently, Eq. (4) has to be modified such that

$$I = (Nf\phi) t \quad (5)$$

The formula of Eq. 5 refers to the idealized case in which all the magnetic field is restricted in a normal region defined by the projection of the pole face on the superconducting sheet. Actually, some field is found outside this projection. The presence of this excess field is explained without difficulty by means of the diffusion of the magnetic

field in a moving conductor is given by

$$\frac{\partial \underline{B}}{\partial \tau} = \nabla \times (\underline{v} \times \underline{B}) + \frac{1}{\mu \sigma} \nabla^2 \underline{B} \quad (6)$$

where μ is the magnetic permeability of the conductor, σ its electrical conductivity and \underline{v} its velocity of translation. By rendering the equation dimensionless one finds

$$\frac{\partial \underline{B}}{\partial \tau} = \nabla \times (\underline{v} \times \underline{B}) + \frac{\nabla^2 \underline{B}}{R_m} \quad (7)$$

where $\underline{v} = \frac{\underline{V}}{V}$ is a unit vector in the direction of translation, the dimensionless quantity R_m is the magnetic Reynolds number defined (6) by $R_m = \mu \sigma v L$ where L is a characteristic length and $\tau = t/(L/v)$ is a dimensionless time referred to the transit time L/v .

The above equation (7) indicates that when $R_m > 1$, the term $\frac{1}{R_m} \nabla^2 \underline{B}$ can be neglected. The equation then simplifies to

$$\frac{\partial \underline{B}}{\partial \tau} = \nabla \times (\underline{v} \times \underline{B}) \quad (8)$$

implying that the fields line appear to be frozen in the conductor.

This is expressed in a different way by noting that

$$R_m = \frac{\mu \sigma L^2}{(\frac{L}{v})} = \frac{t_1}{t_2} \quad (9)$$

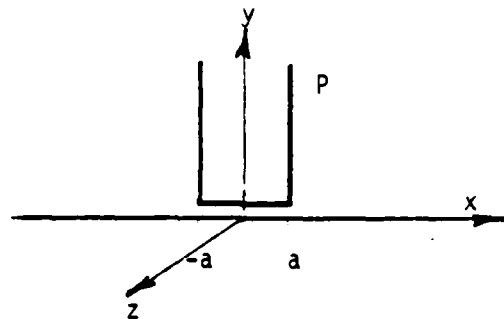
In the above equation t_1 is recognized to be the time of diffusion of the magnetic field in (or out of) a conductor while t_2 as before is the transit time of the normal region with respect to a reference point. Clearly, when $R_m > 1$ then $t_1 > t_2$ and the magnetic field diffuses out of the normal region in a time greater than the transit time of the

region. Under these conditions, the flux pump ceases to function. Volger ⁽⁷⁾ visually observed this phenomenon by means of a Faraday rotation technique. A mirror made from strongly paramagnetic and transparent cesium-phosphate glass was placed on the superconducting sheet. Polarized light reflected from the mirror has its plane of polarization rotated when a magnetic field is present. Thus, it is possible to map the field qualitatively by simply intercepting the reflected light and analyzing it with a polarization filter.

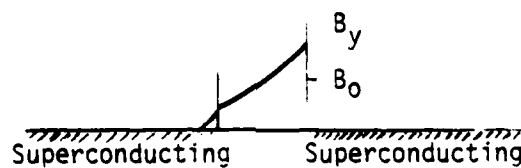
Volger's experiment indicated that as the sheet velocity increased the shape of the normal region developed a "comet tail" as a result of the flux not diffusing fast enough from the region and being trapped in the sheet. An immediate consequence of this trapped flux is to reduce the voltage output from the pump (as ideally expressed by Eq. 2). As the velocity of the sheet is increased, the performance of the pump deteriorates and eventually it stops pumping.

To fix the ideas and derive a quantitative estimate for the performance of the flux pump the distribution of the current and magnetic field inside the moving normal region will be estimated. On the basis of these calculations and by means of the topology of the current path of Fig. 3, an equivalent circuit diagram for the pump will be derived.

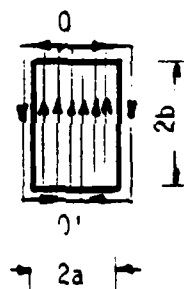
To simplify the mathematics an approximate one dimensional model for the normal region will be used. In this assumption, for steady state and in a frame of reference fixed with respect to the normal region (Fig. 4a),



(a)



(b)



(c)

Figure 4(a) - Frame Of Reference Used In The Calculations. The Frame is Fixed With Respect To The Pole Pieces P Of The Flux Pump.

Figure 4(b) - Distribution Of The y -component Of The Magnetic Field In The Normal Spot. As A Result Of The Magnetic Compression Taking Place, The Field Is Increased At The Leading Edge From The Original (static) Value of B_0 to B_y . At The Trailing Edge, The Field Diffuses In The Manner Discussed In The Text.

Figure 4(c) - Configuration Of The Eddy Current Circulating In The Normal Spot. At $00'$ The Current Is Diverted To The Left And Right In Accordance With Eq. (17).

the sheet will be imagined to be moving to the left with a constant velocity v . The governing equations become

$$\nabla^2 \underline{B} + \mu\sigma \nabla \times (\underline{v} \times \underline{B}) = 0 \quad (10)$$

$$\underline{J} = \sigma (\underline{E} + \underline{v} \times \underline{B}) \quad (11)$$

We now define by \underline{B}_0 the field applied to the sheet, so that

$$\underline{B} = \underline{b} + \underline{B}_0 \quad (12)$$

where \underline{b} is the motion induced magnetic field. Since all quantities are a function of x only, Eq. 10 becomes

$$\frac{\partial^2 b_y}{\partial x^2} - \mu\sigma \frac{\partial b_y}{\partial x} = \mu\sigma \frac{\partial B_0}{\partial x} \quad (13)$$

$$\frac{\partial^2 b_x}{\partial x^2} = 0 \quad (14)$$

It is readily found that

$$b_y = B_0 e^{\mu\sigma v x} 2 \sinh(\mu\sigma v a) + C \quad (15)$$

In the above "a" stands for the half width of the pole piece and C is a constant that must be estimated from the criterion of conservation of flux. Now the conductivity σ becomes infinite for $x > a$, since the sheet in that region is superconducting. The distribution now becomes

$$\begin{aligned} B_y &= b_y + B_0 && \text{for } x > a \\ &= 0 && \\ &= B_0 (1 + 2 \sinh(\mu\sigma v a) e^{\mu\sigma v x}) + C && \text{for } -a \leq x \leq a \\ &= B_0 (2 \sinh(\mu\sigma v a) e^{\mu\sigma v x}) + C && \text{for } x \leq -a \end{aligned} \quad (16)$$

The condition that $\int_{-\infty}^{\infty} B_y dx = 2 B_0 a$ yields the value of C to be $(-\frac{\sinh(\mu\sigma va) e^{\mu\sigma va}}{\mu\sigma va})$. The functional dependence for the field is shown in graphical form in Fig. (4b).

It is noticed that the field component b_y does not vanish in the region $x < -a$ but has a small value. Since the sheet goes from the normal to the superconductivity state in the region $x < -a$ in the presence of a magnetic field whose value is less than the critical field, it is possible for flux to be trapped in the sheet as observed experimentally by Volger.

The distribution of the current in the normal region is readily estimated from Ampere's relation

$$J_z = \frac{\partial B_y}{\partial x} \quad (17)$$

and is shown in graphical form in Figure 4c. The effective resistance and inductance of the eddy current circulating in the normal region can be estimated from energetic arguments. In other words, the effective inductance L_{eff} is found from

$$L_{eff} = \frac{\int_{-\infty}^{\infty} \frac{1}{2\mu} B_y^2 dx}{\left(\frac{1}{2} \int_{-\infty}^{\infty} J_z dx\right)^2} \quad (18)$$

while R_{eff} is defined by

$$R_{eff} = \frac{\int_{-\infty}^{\infty} \frac{1}{2\sigma} J_z^2 dx}{\left(\frac{1}{2} \int_{-\infty}^{\infty} J_z dx\right)^2} \quad (19)$$

The calculations performed above have neglected the fact that the transition from the normal to the superconducting state must include a region in mixed or intermediate state (according to our considering

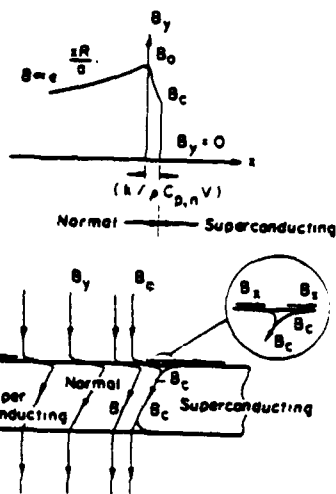


Figure 5 - Accurate Distribution Of Magnetic Field In Leading Edge Of Boundary Layer Of Spot (Ref. 8). The Simple Calculations Derived In The Text And Shown In Figure 4 Have Been Refined To Include The Effect Of Thermal Conductivity (k) Of The Superconducting Sheet. The Lower Sketch Of Figure 5 Shows The Expected Behavior Of The Field In The Thickness Of The Sheet And The Cut-off Of The Field To The Critical Value B_c .

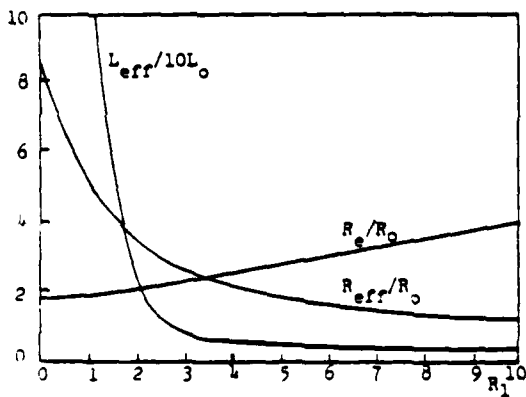


Figure 6 - Dependence Of The Effective Inductance L_{eff} And Resistance R_{eff} Of The Normal Spot As a Function Of The Reynolds Number R_m . The Reference Values L_0 and R_0 Are Given In The Text.

a Type I or Type II material). When this transition is taken into account, the broadening of the boundary layer due to a finite thermal conductivity needs to be taken into consideration.

A more accurate solution for the magnetic field in a normal region was computed (8) and the result is shown in graphical form in Fig. 5.

In Fig. 6, the dependence of the dimensionless quantities L_{eff}/L_0 and R_{eff}/R_0 is given as a function of the Reynolds number $R_m = \mu\sigma v\ell$, where ℓ is the thickness of the current layer. On the other hand

$$L_0 = \frac{\mu b \ell}{a} \text{ and } R_0 = \frac{b}{2\sigma a \ell}$$

where the spot is $2b$ by $2a$ and of thickness ℓ .

On the basis of the observations obtained by us and several investigators and the calculations given above one can draw an equivalent circuit for the flux pump, shown in Fig. 7, includes most of the salient features of the flux pump. In particular, it can duplicate the decline of the output voltage of the pump after a maximum is reached. The maximum which is fixed by the rapidity of the diffusion of the magnetic field out of the material corresponds to $R_m = 1$.

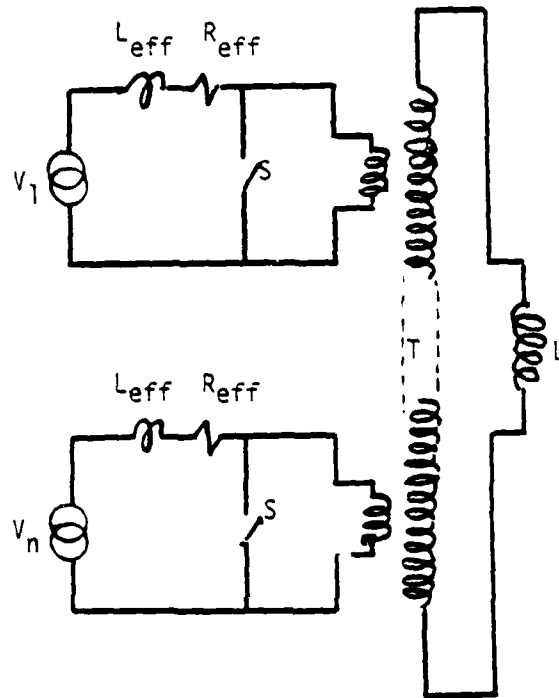


Figure 7 - Equivalent Circuit Diagram For Flux Pump. Each Spot Is Akin To A Generator V_n , With An Internal Inductance of L_{eff} and resistance R_{eff} . The Switch S Normally Short Circuits The Generator And The Corresponding Short Circuit Current Is The Eddy Current. When The Spot "pumps", The Switch S Is Opened And The Flux Is Inductively Linked To The Load Coil L . This Operation Is Performed Through The Idealized Transformer T .

SECTION III

CONSTRUCTION FEATURES OF GENERATOR

The general appearance of the generator is shown in schematic form in Figure 8. This drawing is helpful for the purpose of visualizing the location and role of various components of the generator.

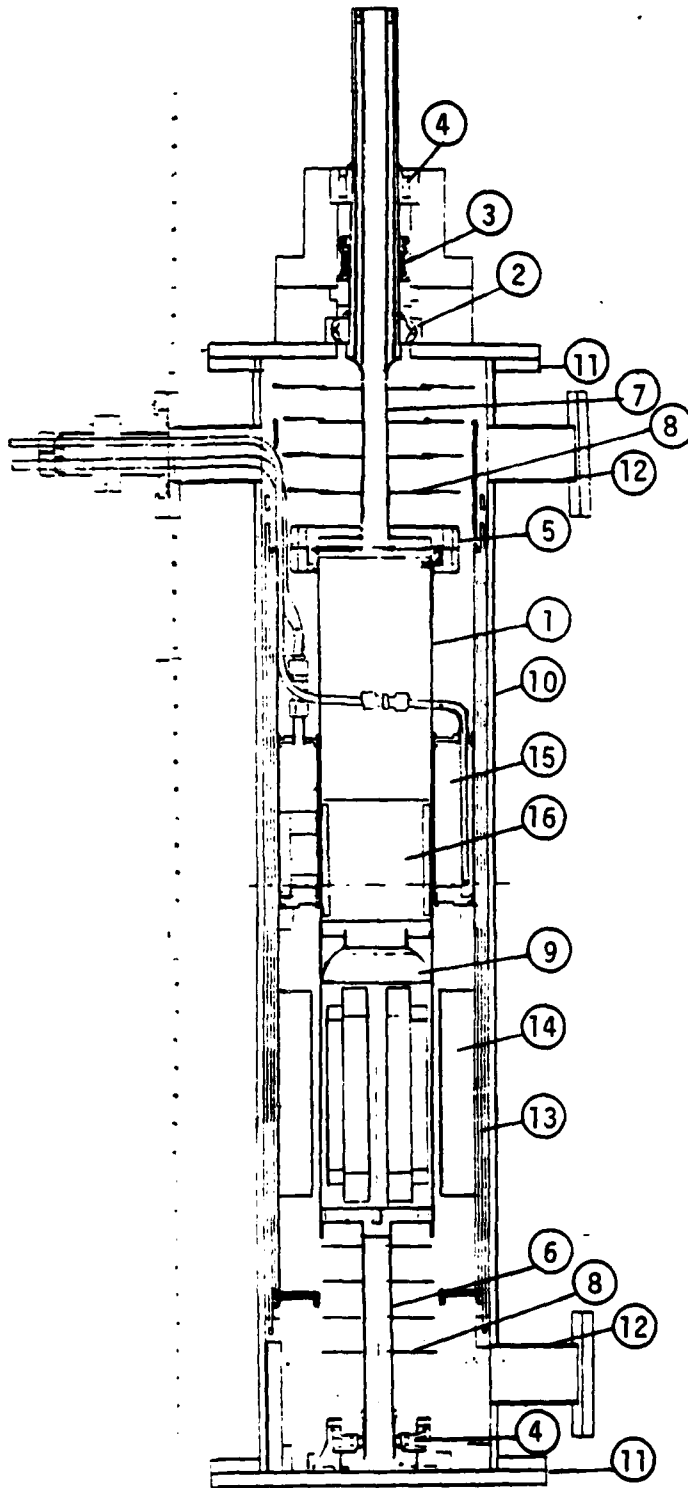
The design of the generator calls for detailed calculations of the armature, the field windings, the flux pump, the cryogenics and the mechanical characteristics of various components: rotating seal, shield, insulated supports, etc... The starting point of the design is the determination of the key dimensions of the generator. These are the diameter of the field windings, length of rotor and length and diameter of rotor shaft.

1. Rotor - Dewar

One of the main considerations in the selection of the diameter of the rotor was the availability of seamless stainless steel pipes in the vicinity of four inches. This size was chosen to keep the cost of the generator low and within the limits of our budget. The nearest standard size turned out to be 4" OD. (1 on Figure 8)

Once the size of the rotor was fixed, the length of the rotor was selected on the basis of two considerations. The first required that the volume of the rotor be large enough to store an adequate amount of liquid helium, the second was the concern for the onset of unwanted whirling vibrations which might take place because of the slender shape of the rotor.

A difficulty that was encountered with our first model of the superconducting alternator (9) was due to the rotating vacuum seal losing its integrity when the system was cooled down to liquid Helium temperature. This



- ① rotor casing
- ② thrust bearing
- ③ rotating seal
- ④ ball bearings
- ⑤ con-flat flange
- ⑥ lower shaft
- ⑦ upper shaft
- ⑧ radiation shields
- ⑨ field coil former
- ⑩ stator (main) casing
- ⑪ main flanges
- ⑫ connecting ports
- ⑬ liquid N₂ jacket
- ⑭ armature coils
- ⑮ liquid N₂ magnet casing
- ⑯ flux pump

Figure 8 - Engineering Details For Superconducting Brushless Generator Described In Report.



Figure 8a - General View Of Generator, Together With The Vacuum And Cryogenic Systems.



Figure 8b - Photograph of Vacuum Vessel.

malfunction was due to the differential contractions of several parts of the system. To avoid the occurrence of this effect, the rotor was suspended from a thrust bearing (2 on Figure 8). Any contraction taking place would keep the relative separation of the vacuum seal unaffected. Our decision turned out to be a correct one since the vacuum obtained was very good. The rotating vacuum seal was a John Crane seal model 15 WT and placed just above the thrust bearing (3 on Figure 8).

To provide alignment for the dewar, two additional roller bearings were added: one above the rotating vacuum seal and the other sliding type at the bottom (4 on Figure 8). This configuration led to the fundamental whirling frequency to be around 1100 rpm. Since the design called for a rotation at 500 rpm, there was an ample factor of safety.

Since we wanted to provide flexibility to the construction of the dewar, in particular to be able to open the dewar either for inspection or for alteration, the original idea to have the rotor completely welded was changed. The top part of the dewar (5 on Figure 8) was constructed out of Varian Conflat flanges. Although the specifications provided by the manufacturer guaranteed the flanges only to liquid Nitrogen, we found that by careful machining, the flanges could be extended to an operation range at liquid Helium temperature.

It was essential to minimize the thermal losses by conduction from the rotor in spite of the actual solid to solid contacts at the bearings. Accordingly, the bottom stainless steel shaft of the rotor (6 on Figure 8) was made as thin as possible and was further perforated with many holes to effectively increase the thermal resistance.

Similarly, the top shaft (7 on Figure 8) was constructed out of thin stainless steel tubing. A slightly larger diameter tubing is concentrically welded at the top to provide vacuum between the two tubings. The vacuum layer cuts back on the conduction losses. Whenever physical contacts were needed to provide stiffness and increased mechanical strength to the shaft, the same approach as used in the lower shaft was simulated, *viz.*, the cross section of the member making the contact was reduced as much as possible.

Another point needs to be mentioned. The complex structure of the top shaft was used not only to diminish the thermal losses, but also to avoid the silicone oil of the rotating vacuum seal from being cooled to too low a temperature as to cause it to freeze. Our design turned out to be most effective since the silicone oil was kept at a temperature very close to room temperature.

The estimated heat losses from the rotor by conduction were 200 mW. To cut back on the radiation losses from the rotor, the outside surface of the rotor was polished to a high degree. On the other hand, radiation shields attached to the shafts (8 on Figure 8) played the important role of reducing the radiation losses from the ends of the rotor-dewar.

2. Field-(Excitation) Coils

The magnetic field intensity in the air gap of the machine bears a direct relation to the ampere-turns of the excitation coils and to the width of the air gap. There was a great advantage to reduce the air gap as much as practical to lower the reluctance of the flux path. The width was actually set by the thickness of the rotor-dewar as well as by the physical air gap which had to be kept to a reasonable dimension to account for misalignment in

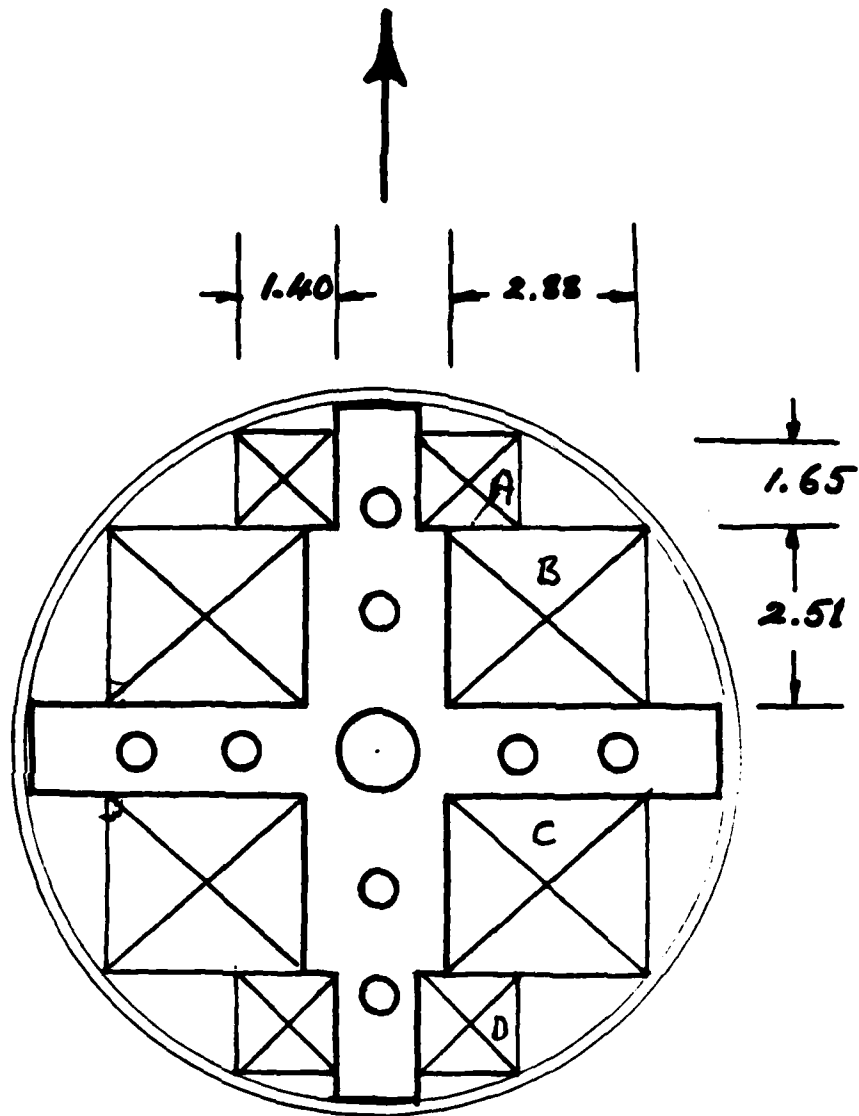


Figure 9 - General Layout For Superconducting Field Coils.
 All Dimensions Are In cms. The Drawing Is Full
 Scale.



Figure 9a - Photograph Of Field Coils Mounted On Former

in the construction. Actually, our construction tolerances were good enough that the physical gap was made 5 mm.

A second consideration was then given to the distribution of the magnetic field in the gap. Should we have made a distribution which was as close to uniform as possible? The peak value of the field intensity would have been low, since the volume available for the winding is finite. Accordingly, we decided to aim for a triangular like distribution in the gap. A result of such a distribution is to lead to many harmonics in the output. It does, however, have the advantage of yielding a higher peak field in the gap.

The configuration for the coils is shown in Figure 9. Since it was desired to demonstrate the ability of the flux pump to reach currents of 1000 amps., the conductors that were selected had the following characteristics:

Superconducting material	Niobium Titanium
Configuration	Rutherford Stranded Cable
Cross Section	.125" x .041"
Number of wires	13
Individual wire diam.	.020"
Number of twists per inch	2
Cu to supercond. ratio	1.8:1
Number of filaments per individual wire	2200
Individual filament diam.	6.3 micron
Insulation	Formvar.

The coils were wound for us at Magnetic Corporation of America and according to the specifications we provided. The conductors were barber pole wrapped

with epoxy impregnated fiber glass tape prior to winding the coils. After winding, the field coils were baked for a few hours in an oven. The tapes thus were cured and caused neighboring turns of the coil to adhere very firmly to each other.

The field coils were then mounted on an Aluminum former which had been drilled with holes to reduce its mass and to allow the free flow of liquid Helium in the coil. The location of the former is shown as 9 on Figure 8.

The coil was braced to the former by means of wide fiber glass tape which tightly encircled the coils. The base of the former was attached to the inside of the rotor by means of bolts. The combination fitted snugly in the rotor so that there was no chance for the coils to "rattle" in the rotor.

3. Flux-Pump

The flux pump was the most crucial component of the generator in that it had to be designed so as to meet the special requirements of current capacity, speed of pumping, rotational rate per minute and compactness.

The flux-pump construction incorporated a number of improvements and innovations. The general appearance of the pump is shown in diagrammatic form in Figure 10, (also 16 on Figure 8).

The first of these improvements has to do with cooling of the pump. Upon rotation of the rotor-dewar the liquid Helium inside it will also rotate. Consequently, the free surface of the Helium will be curved in a meniscus-like configuration. An immediate consequence of this effect is that the central portion of the pump, as well as, the wires connecting the output of the pump to the field coils below it, will be exposed and hence will not be cooling.

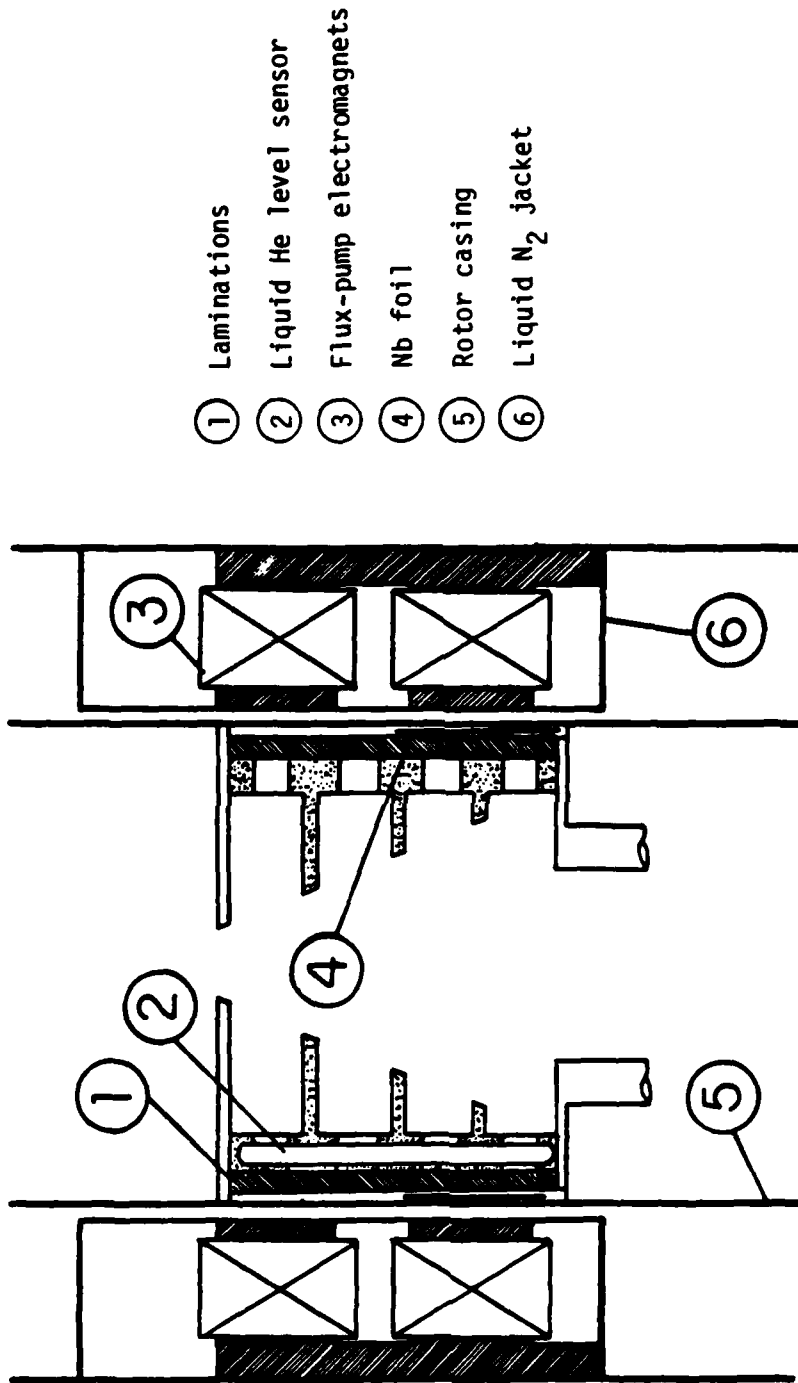


Figure 10 - Schematic Diagram For Flux Pump

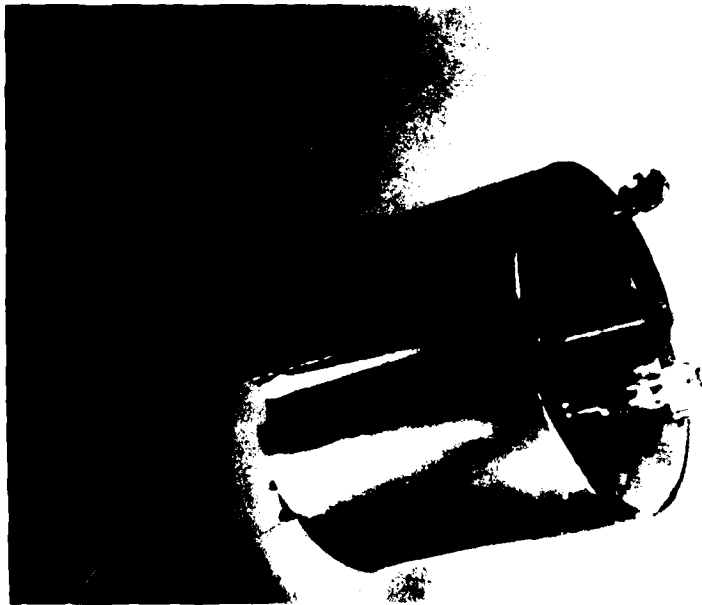


Figure 10a - Photograph Of Nitrogen Cooled Electromagnets
For Flux Pump.

To avoid this difficulty, mock-up experiments were conducted in which it was ascertained that the addition of several baffle like plates introduced in the core of the pump (see Figure 10) tend to break the meniscus and trap the liquid between them. As a result, the meniscus forms on top of the pump. The pump and the field coils thus remain immersed in and wetted by the helium for as long as the helium lasts in the rotor.

A second addition in the design was the use of iron laminations for the return path of the exciting field. The laminations were stamped with an extension so that the stack of laminations were kept very firmly in place by two stainless steel reings which had a groove milled in them. The orientation of the laminations were such as to minimize the eddy current losses in them. When the laminations are mounted, they form a cylindrical shell which rests on a micarta skeleton.

A niobium foil, which is the heart of the pump and which is two inches wide and 0.5 mil. thick, is then wrapped once on the laminations which had been covered with a perforated mylar film. Twelve NbTi conductors are spot welded on each edge of the Niobium sheet. Each bundle of conductors are then brought to a common contact that forms one of the terminals of the pump. The excitation coil leads are soldered to these terminals. A perforated sheet of mylar is wrapped around the Nb foil for protection.

All leads and the pump are firmly attached to the field coils so that the combination of pump, former and field coils are one unit which can be bodily inserted in (or removed from) the rotor-dewar.

To check the theory of operation of the pump and to provide diagnostics for the determination of the characteristics of the flux pump, a

variety of sensors were inserted in the flux pump. These consisted of the following:

- 1) a liquid Helium level indicator. The flux pump is the first of the generator elements to become exposed as the Helium level drops. Accordingly, a short (10 cms) indicator manufactured by American Magnetics, Inc. was fitted inside the micarta body of the pump.
- 2) a current transformer was installed in a groove in the micarta frame. Details are given in the section on Instrumentation.
- 3) a few lengths of wires placed on the niobium foils and electrically insulated from it. These dummy wires act as pick-up coils. The purpose of these sensors is to clarify the ongoing processes in the flux pumping. A point which still remains to be explained is the dependence of the pumping rate on the number of leads. In principle, there should not be any dependence, but preliminary observation shows it otherwise. These observations do not seem to be very certain and more careful measurements need to be made.

SECTION IV CASING AND STATOR

The casing of the machine contains the stationary parts of the alternator. In the original design the compactness was considered to be one of the essential goals. For this a brass tubing, 8 inch O.D. and 40 inches long, with a wall thickness of 1/8" was used (10 on Figure 8). Two brass ring flanges (11 on Figure 8) were machined and silver soldered to the top and bottom of the tubing. Three extension arms, 2 inches in diameter, were silver soldered near the top of the casing for various input connections. A similar single outlet port was used near the bottom of the casing. Brass machined flanges were silver soldered

to all these outlets (12 on Figure 8). The casing was vacuum tested for vacuum leaks before assembly. Double O-rings were used for outlet flange connections. For the top and bottom flanges, Grafo-seals were also used in addition to O-rings to insure leak free operation during the machine tests.

In order to reduce radiation leaks between the rotor at 4.2⁰K, and the casing at room temperature, a specially constructed liquid N₂ jacket was inserted between the two (13 on Figure 8). The jacket was made up of two brass tubes. The outside and inside diameters of the jacket were 7.5 and 7.0 inches respectively. To reduce the heat leak further, the outside of the liquid N₂ jacket and inside of the main casing were lined with Aluminum foil. The gap between the two was 1/8" after assembly. The liquid N₂ jacket was supported by Micarta legs which are fastened to the bottom flange. Small Micarta inserts were also used at the top to avoid accidental contact of the jacket with the casing. Four brass lugs were silver soldered to the inside of the liquid N₂ jacket to be used for support of the magnets and the stator coils.

Two 1/4 inch copper tubes were silver soldered to the top and bottom of the liquid N₂ jacket for liquid N₂ connections. These tubes were brought up to the top of the jacket and two stainless-steel Swageloks were silver soldered to them for assembly purposes. A liquid N₂ feed through with con-flat flanges were adapted for outside liquid N₂ connections. The system was then vacuum leak tested by running liquid N₂ through the jacket and by evacuating the casing.

1. Armature Coils

The major goal of the experiment was to demonstrate the charging and discharging of the field coils of the generator utilizing the flux-pump. The power output of the device at that time was of secondary importance. Thus, no extensive design of the stator coils was undertaken. Just to show that the generator puts out generated voltage, two coils were placed across the field coils (14 on Figure 8). These stator coils were wound by using a special jig and former. They are attached to the inside of the liquid N_2 jacket using proper micarta brackets. The outputs of the stators were brought out separately using the feed-throughs on one of the output flanges.

2. Flux-Pump Magnets

Flux pump magnets had to be designed to satisfy the necessary requirements for successful operation of the flux pump and the generator as a whole. Since Nb foil was used in the flux pump, the following magnet characteristics had to be satisfied:

- a) The magnetic field at Nb foil should be greater than 0.18 Tesla to turn the foil to its normal state. Since the amount of flux pumped is proportional to the magnetic field strength, magnetic field intensities up to 0.6 Tesla were considered.
- b) Because of the space limitations and rotating field configuration for rotor, the magnets had to be placed outside the rotor. Thus, an air gap larger than anticipated had to be used in the magnetic circuit as shown in Figure 10. Here, the air gap was made up of the space between the magnet pole and the rotor tubing, rotor tubing thickness, Nb foil

and the corresponding electrical and thermal insulating materials. Minimum overall gap was taken to be at least 5 mm which introduced a larger reluctance for the magnetic field. Since the same gap had to be incorporated for both pole faces, the effective gap was greater than 10 mm. The magnetomotive force necessary to produce the required field at the gap was mostly expended at the air gap provided the magnetic materials did not saturate.

- c) The maximum space between the liquid N₂ jacket and the rotor is 1.5 inches. This space restriction puts limitations on the amount of magnetic material that could be used in the magnetic circuit. Thus, design parameters dictated magnetic materials to be used near their saturation limits.
- d) One of the theoretical predictions of the flux pump theory is the necessity of sharp magnetic field boundaries. Having an air gap of about 4.5 mm between the pole faces and the superconducting Nb foil, it became necessary to use a magnetic material for the flux return path. This path is made up of laminations cut from a transformer steel sheet. Because of space limitations in the rotor, the depth of these laminations were restricted to 6 mm. Limited cross sectional area and possible saturation of the laminations reduced the maximum available field strength at the gap.

Six electromagnets were constructed using a commercially available magnetic material. The pole pieces were machined from a plate 10 mm thick and the pole faces had a cross sectional area of 10 mm x 25 mm. The coils were wound from #26 gauge wire having 3000 turns each and were thoroughly baked after immersing them in shellac insulation.

The magnetic field profiles are measured using a magnetic configuration similar to Figure 10, but due to rapid heating of the coils at full design current of 600 mA, smaller excitation currents were used for tests. From these measurements it was concluded that the required fields would be obtained at the rated current.

When the system was assembled and without cooling process initiated, it was found that the maximum field attainable at the gap was around 0.2 T which was just above the critical field of the Nb foil. When attempts to increase the field were tried by increasing the excitation current, the coils began outgassing due to ohmic heating. This had a detrimental effect of increasing the casing pressure which immediately led to a very high conduction losses in the vacuum chamber. Detailed analysis showed that the commercial magnetic material saturated at magnetic field intensities around 0.8 - 1.0 Tesla. Thus, it was impossible to increase the magnetic field across the air gap to the design value of 0.6 T.

An attempt was made to run the alternator with the assumption that if the field coil currents were increased to 3 ampere and after 1 or 2 minutes they were de-energized, a short run would be possible. A complete run of the system was tried with liquid Helium filling of the rotor, but as soon as the currents were turned on, the outgassing was very fast. Each coil consumed about 225 watts of electrical power. Pressure in the casing increased very rapidly, evaporating the liquid Helium in the rotor. With this arrangement, it was not possible to get any coherent data out of the system. Negative results obtained using the commercially available magnetic material forced us to design a new completely different electromagnet system.

The second generation of magnet design was based on enclosing the magnets and coils in a liquid N_2 jacket (15 on Figure 8). This concept:

- a) avoids any possibility of outgassing by the coils
- b) insuring that the magnets will remain nearly at liquid N_2 temperatures even if the coils were over-excited, thus, maintaining the same temperature difference between the rotor and the coils.

An extensive design of the new magnets started by obtaining reliable magnetic steel for the cores from Sterns Magnetics. The geometrical shape of the magnets was changed to reduce the saturation effects of the flux pump laminations. With the six magnets and the requirement that the magnets do not effect their neighbors, an effective pole face of 2.0cm was chosen for each magnet. To ensure that the measurements were taken with the full exciting magnet currents under the actual experimental conditions, the flux pump laminations were incorporated in these measurements using a special fixture that introduced an air gap of 5 mm between the magnet poles and the laminations. A hall probe was inserted in the air gap to measure the magnetic field. Two sets of experiments were done. First of all, the whole system was immersed in a liquid N_2 dewar and increase of B field vs excitation current was recorded on an X-Y recorder. Current and voltage measurements that were taken during this time showed that the resistance of the coils dropped an order of magnitude from room temperature values by immersing them in the liquid N_2 . The power dissipated for each coil was around 25 watts at full excitation. The excitation continued for about half an hour and no noticeable changes in the field, coil current and excitation voltage were observed. The second set of experiments were based on measurement of the magnetic field profiles. This was done by

using a motorized moving hall probe. These experiments took place at room temperature. Although the temperature of the coils (600 turns total for this design, 400 turns across Nb foil and 200 turns across the other pole) increased slightly with time, a current regulator maintained constant excitation current during the traversal of the hall probe across the pole faces. Typical field profiles, field versus excitation current and stability of field with time are shown in Figures 11 & 12. With this new design, the magnet system was able to produce magnetic fields in excess of 0.6 T at the gap with the required sharp magnetic gradients.

The six magnets were enclosed in a specially machined stainless-steel casing. This time the liquid N₂ feed-throughs were specially designed and custom made to accommodate one 1/4 inch inlet tubing and two 3/8 inch outlet tubings. The electrical leads for the magnets were brought out through the outlet tubings eliminating special electrical feed-through and assuring cooling of the wires by the exhaust liquid N₂ vapor. The magnet casing was fixed to the main liquid N₂ jacket through the special lugs that were silver soldered to the jacket.

3. Vacuum System

Evacuation of the system was done by using a liquid N₂ trap, oil diffusion pump and a mechanical pump. Pressures around 10⁻⁵ Torr were maintained in the system during the cooling cycle and rotation of the rotor. Two thermocouple gauges and one vac-ion gauge were used to monitor the pressure constantly.

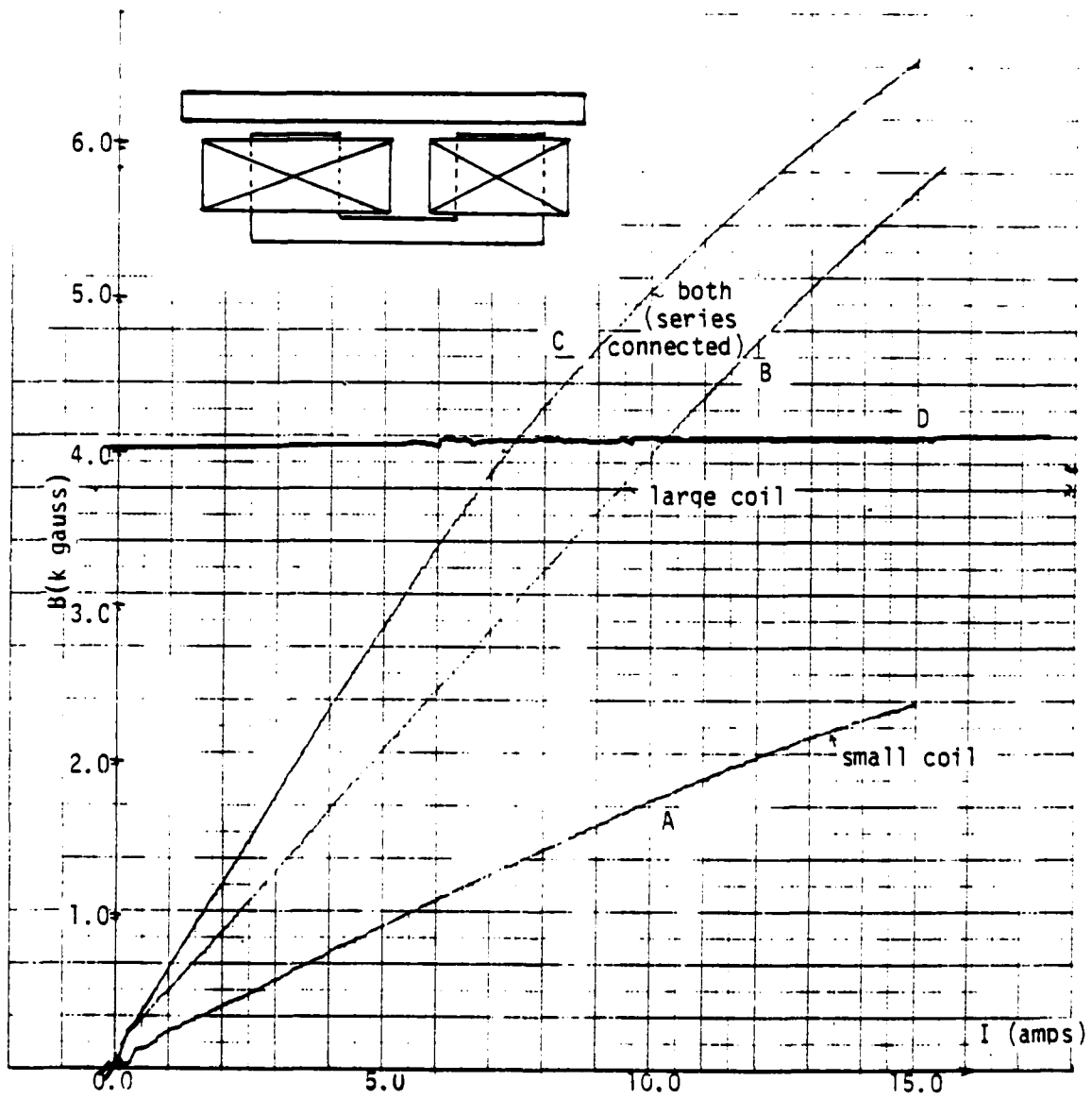


Figure 11 - Magnetization Curves For Electromagnets Used In The Excitation Of The Flux Pump. Since Each Electromagnet Had Two Exciting Coils, The Magnetization Curves For The Use Of One Or Two Coils Is Shown Above.

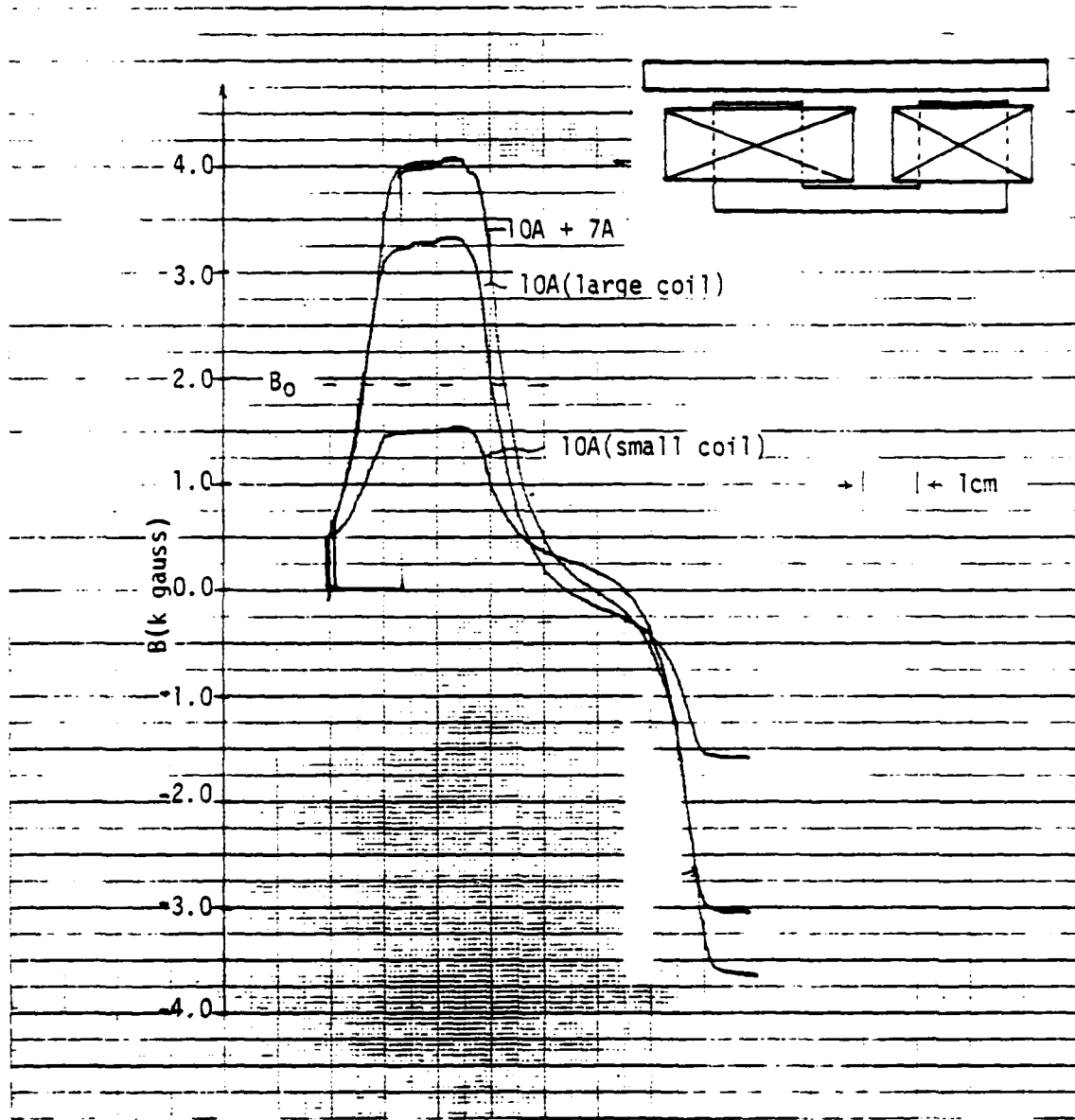


Figure 12 - Magnetic Field In The Air Gap Of The Flux Pump For Different Excitations Of The Electromagnet. These Various Tests Were Conducted To Verify The Independence Of The Sharpness Of The Field Distribution As A Function Of Field Strength.

SECTION V INSTRUMENTATION

Detailed measurements of the various parameters of the generator were required for experimental verification of the operational characteristics of the flux-pump and the alternator. Toward achieving these goals, the instrumentation had to be incorporated into the rotor system as well as the usual stationary instrumentation associated within the stator casing.

The following instrumentation was used for various diagnostic purposes:
(Referring to Figure 13 for locations)

1. Stator
 - a) Hall probe to measure the magnetic field produced by the field coils.
 - b) Output voltage generated by the generator.
 - c) Temperature diode to measure the cooling cycle.
 - d) Thermocouple gauge to monitor the pressure.
 - e) Ion gauge to monitor the pressure.
2. Rotor
 - f) Hall probe placed just beyond the Nb coil to monitor the magnetic field variations of the flux pump.
 - g) 4" liquid Helium level sensor. Monitors the liquid Helium level in the rotor while the experiment is in progress.
 - h) leads to monitor the induced currents and voltages across the Nb foil.
 - i) Current transformer to measure the build-up of current in the field coils.

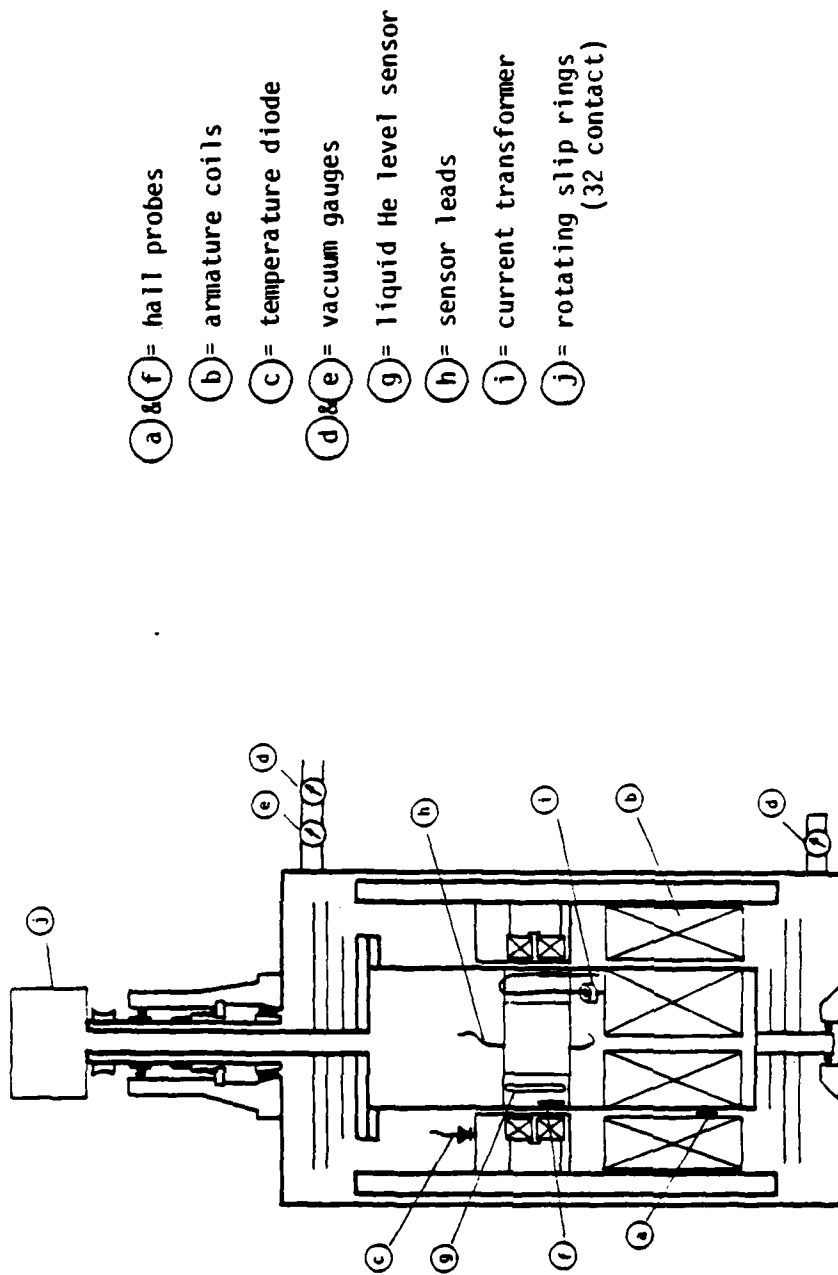


Figure 13 - Schematic For The Location Of The Sensing Devices Referred To In The Text.



Figure 13a - Photograph Of Flux Pump And Field Winding Showing Location Of, And Connections To The Sensors.

Special precautions are taken in the instrumentation of the current buildup. It was decided not to break any portions of the superconducting loop by introducing non-superconducting instrumentation in series with the superconducting loop made up of the field coils and the Nb foil of the flux pump. For this a special current transformer was designed based on the principle of flux generated around a current carrying conductor (Figure 14). A low temperature Hall probe was used to measure this flux. Calibration of the current transformer was made at liquid N₂ temperatures by using rated currents for short durations. In the rotor, the transformer is placed inside the flux pump. The superconducting leads coming out of the Nb foil were brought to the location of the transformer and after passing all of them through the transformer, the soldered connection to the field coil was made.

- j. A 32 contact rotating slip ring was used to bring all these various diagnostic leads out of the dewar.

SECTION VI ASSEMBLY OF THE GENERATOR

Although the generator was designed to be as compact as possible and the rotor and stator were considered to be two separate units, the limited space availability between the stator flux pump magnets and the rotor required very careful step by step assembly of the generator. One of the main difficulties in the assembly was the connections that had to be made between various liquid N₂ input and exhaust feed through with the tubings coming out of the Liquid N₂ jacket and the liquid N₂ magnet container of the flux pump.

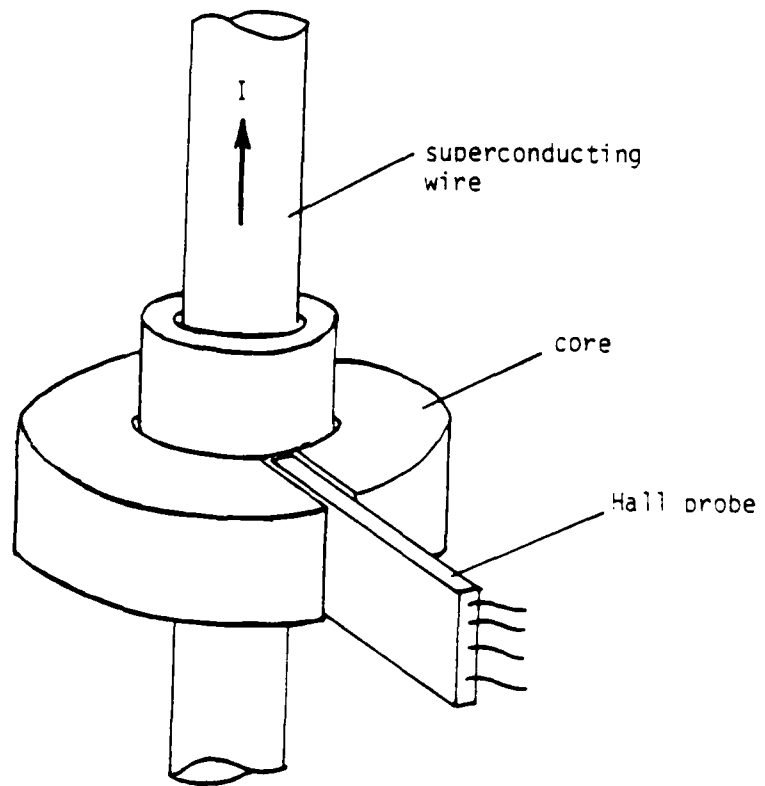


Figure 14 - D.C. Current Transformer Used To Measure The Flux Pump Current.

SECTION VII COOLING AND OPERATION

The following procedures were followed in cooling and operation of the generator:

- a) System was evacuated.
- b) Main liquid N₂ jacket was filled with liquid N₂.
- c) Magnet casing was filled with liquid N₂.
- d) Liquid Helium is transported from 100 liter liquid Helium storage dewar.
- e) Liquid Helium level was constantly monitored by a liquid Helium sensor attached to the liquid Helium transfer line.
- f) Once the dewar was filled, the transfer line was removed, rotating slip rings were placed at the top of the rotor and the electrical motor was activated to bring the rotor to the rated rpm.
- g) Flux pump magnets were turned on and measurements were taken.

SECTION VIII MEASUREMENTS AND RESULTS

Two sets of measurements were performed: static measurements in which the generator was not activated and dynamic measurements related to the checking of the generator characteristics.

1. Static Measurements

Most of these measurements have been performed by means of conventional procedures. All the pertinent data have been compiled here for convenience.

a) Superconducting Coils

Dimensions: Four coils stacked as shown in Figure 9. The overall dimensions for the two larger ones are 20 cm long, 7.76 cm wide and 2.50 cm deep. The two smaller coils are 20 cm long, 4.30 cm wide and 1.65 cm deep.

Inductance: The total inductance for the four coils in place on former and connected in series is 3 mH.

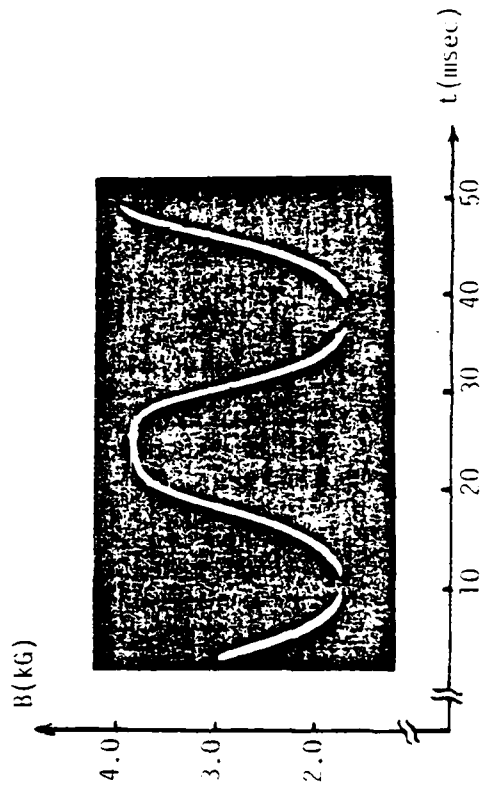


Figure 15 - Dynamic Measurement Of The No-load Magnetic Field In The Air Gap Of The Flux Pump

b) Stator Coils

Dimensions: Two saddle shaped coils with an overall dimension of
22.5 cm by 13.75 cm.

Inductance: 37.29 mH

Resistance: 39.9 Ohms

c) Flux Pump Electromagnets

The actual distribution of the magnetic field in the air gap (is shown in Figure 15) the rotor was in place and cooled down to liquid nitrogen temperature so the flux pump was not operating. The field was detected by means of a Hall probe inserted in the rotating dewar. The maximum value of the magnetic field in the case shown in Figure 15 is 4 kGauss. The normal working field in the airgap is 4 kGauss.

2. Dynamic Measurements

The main goals of these sets of measurements were to demonstrate the feasibility of the brushless superconducting generator. In particular, the specific characteristics that needed to be tested were

- a) The ability of the flux-pump to "charge" and "discharge" the field coils.
- b) The ability of the field coils to maintain the field coils current, while the generator was in motion. In other words, one needed to check whether the superconducting coils did behave as permanent electromagnets once the flux-pumping ceased.
- c) The determination of the pumping rate - in the charging and discharging cycle - and the dependence of the pumping rate on the strength of the magnetic field and on the speed of rotation.

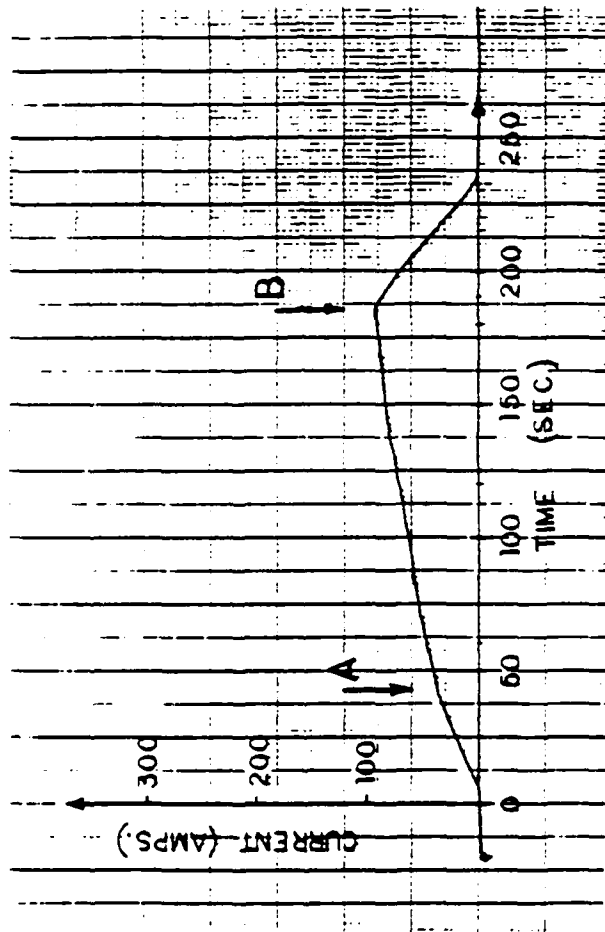


Figure 16 - First Trial Histogram For The Build-up Of The Current In The Field Coils. At The Point A, Overheating Of The Foil Caused The Superconducting Foil To Quench. Between A and B The Flux Pump Functioned As A Conventional Homopolar - At B The Pump Field Was Reversed So That The Coils Were Discharged.

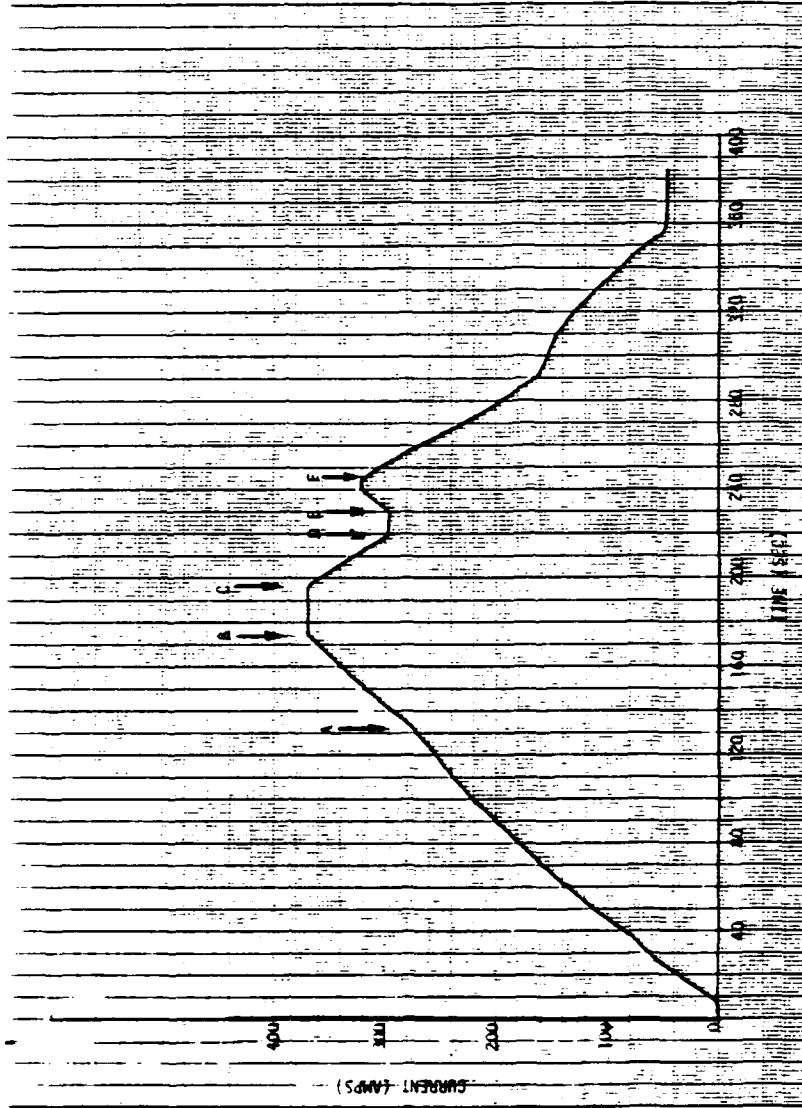


Figure 17 - Typical Histogram Demonstrating The Ability Of The Pump, To Go Through The Various Modes Of Operation As Expected. Between 0 And A, The Speed Of Rotation Was Increased In Steps. Between A And B The Speed Was Constant. Between B and C The Flux Pump Was Turned Off And The Coil Held The Current. Between C And D The Pump Field Was Reversed, at D The Pump Was Turned Off, At E It Reversed, At F It Was Reversed Again And During This Discharge Phase The Speed Of Rotation Was Reduced In Steps Three Times.

- d) The determination of the maximum current that was reached in the field coils and the comparison of this value with the theoretical limit.
- e) The determination of the induced pumping voltage across the field coils.
- f) An evaluation of the losses in the flux pump.
- g) The determination of the output voltage.

a. Histogram of Field-coils Current

In one of the earliest tests made, the temporal behavior of the field current followed a typical behavior similar to that shown in Fig. 16. The magnetic field in the air gap of the flux pump was 4 kGauss, and the rotor was spun at 300 rpm. The current first increased at the rate of approximately 1.1 amps/sec, then after 30 secs, the charging rate suddenly dropped to the value of 0.5 amps/sec. Furthermore, the charging was no longer linear. Upon reversal of the field of the flux pump, the pump was able to discharge the coils, but at the faster rate of 2 amps/sec. This behavior was quite consistent and could be duplicated many times.

This disappointingly low value of the pumping rate, as well as, the sudden change of the rate was very puzzling. Careful checking of the heat dissipation in the flux pump indicated that the flow of liquid Helium around the niobium foil was not adequate. As a result, the foil was quenched to the normal state of the heating in the presence of the high magnetic field. The flux pump, therefore, operated as a homopolar generator with a corresponding low value of the charging rate.

Redesign of the cooling in the flux pump, remedied this situation. The histogram of Fig. 17 clearly demonstrates that the charging rate is higher.

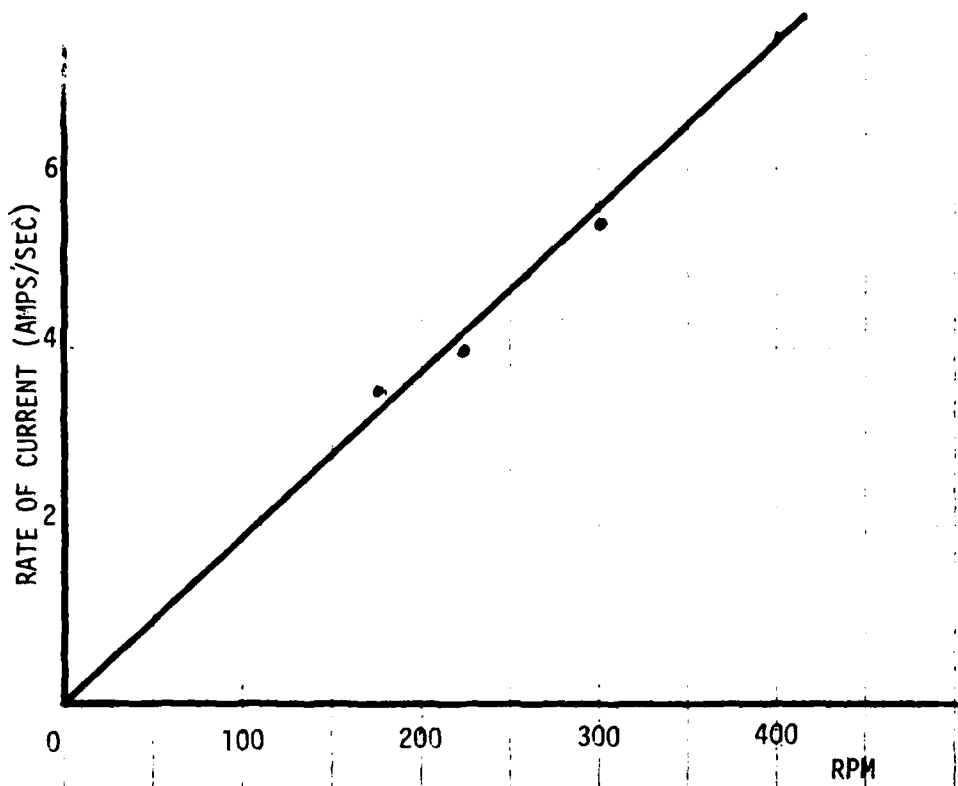


Figure 18 - Dependence Of The Rate Of Charging On The Speed Of Rotation

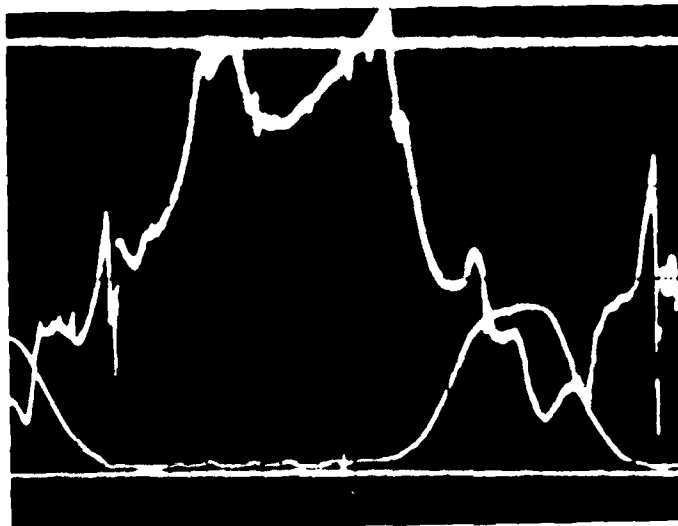


Figure 19 - Temporal Dependence Of The Voltage Induced Across The Superconducting Belt. Each Square Corresponds To 20 msec. The Ripples Are Due To Slots In The Laminations Of The Pump.

It also shows that the rate increases linearly with the rotation speed. For the sake of comparison with the results reported in Fig. 16, the rate is 5.6 amp/sec at 300 rpm. If the generator had been rotating at 3000 rpm, the rate would be 56 amps/sec and had its speed been increased to 10,000 rpm the rate would escalate to 184.8 amps/sec. The dependence of the rate of charging on the speed is shown in Fig. 18.

The histogram of Fig. 17, also indicates, that the field coils can hold the current and that the rate of discharge is the same as the charging rate as it should be.

b. Behavior of Induced Voltage

The oscillogram of Fig. 19 shows the potential difference across the leads of the field windings as a function of the time. The envelope of these signals roughly resembles the distribution of the magnetic field in the air gap of the flux pump.

The ripples on the curves are caused by slots in the laminations behind the niobium sheet which were placed there to allow for the passage of the leads that are periodically spot welded on the Nb sheet. As a result, the local magnetic flux through the normal region is modulated because of the variable magnetic reluctance due to these slots. In a working generator, these slots are avoided. Here, they were introduced for the ease of construction.

The periodic pulses shown in Fig. 19, represent the voltage referred to in Eq.(2). It, therefore, is consistent with the model in which the flux associated with the field windings is increased by small steps and at a frequency of Nf (N is the number of poles and f the frequency of rotation).

If we denoted by V_{av} , the mean value of this induced voltage and if $I(t)$ is

the instantaneous value of the current in the field coils, the total work expended in charging the coils is

$$W_m = \int_0^T V_{av.} I(t) dt \quad (20)$$

Where T is the charging time. Of course, if the final current is I_{max} , then we also have

$$W_m = \frac{1}{2} I_{max}^2 L \quad (21)$$

with L being the inductance of the coils. The maximum current that was measured was 380 amps. Consequently, the energy stored in the field coils at that value of the current is 218 joules.

3. Energy Losses in the Flux Pump

To evaluate the losses in the flux pump one must know the value and distribution of the current circulating in the normal region (i.e. the eddy currents). The direct measurement of these currents is extremely difficult.

A very good estimate of the value of this current can be had from a simple approximation which goes this way*

$$I = \frac{Bv(2b)}{R} \quad (22)$$

where R is the ohmic resistance of one region.

The energy losses in the pump are therefore

$$W_{loss} = N \frac{(Bv(2b))^2}{R} T \quad (23)$$

As before, T is the time required to reach maximum current, N is the number of poles and (2b) is the height of the magnetic spot.

* This is simply derived by equating the induced voltage to the ohmic drop in the eddy.

When one calculates the losses as expressed by Eq. (-3) for a sheet 0.5 mil. of niobium at 4.2⁰K, it is found that

$$T = 100 \text{ secs} \qquad v = 3.14 \text{ cm/sec}$$

$$B = 0.4 \text{ Tesla} \qquad 2b = 2 \text{ cm}$$

$$R = 2.52 \times 10^{-6} \text{ ohms}$$

$$W_m = 218 \text{ joules}$$

$$W_{\text{loss}} = 15 \text{ joules}$$

which yields an efficiency of about 93% for the pump. Considering, that the material used was not optimum, one readily concludes that if the niobium is replaced with a Pb-In or Pb-Bi alloy, the resistivity of the sheet and the efficiency can be enhanced considerably.

4. Maximum Pump Current

The original design of the field coils allowed for a maximum current of 1000 amps. When the tests were performed, it was observed that the maximum current that could be reached was a little under 400 amps, at which point, the sheet quenched to the normal state.

This expected limitation was finally explained by noting that in the original design of the pump, the Nb sheet was supposed to be two inches wide. (5 cm approx.). To improve the cooling, various passages were introduced to allow for the free flow of Helium. The sheet had thus to be made narrower by almost one cm. An immediate consequence of this narrowing was to restrict the total current, in the vicinity of the leads, to a narrow strip so that the local value of the self magnetic field rose to a value equal to the critical field for Nb (0.1920 Tesla) causing the sheet to quench. To remedy this situation, one should replace the sheet with a wide one (at least 1 cm more) or welding a thick rim of NbT₃ at the edge. This requires a radical change in the construction which is not warranted.

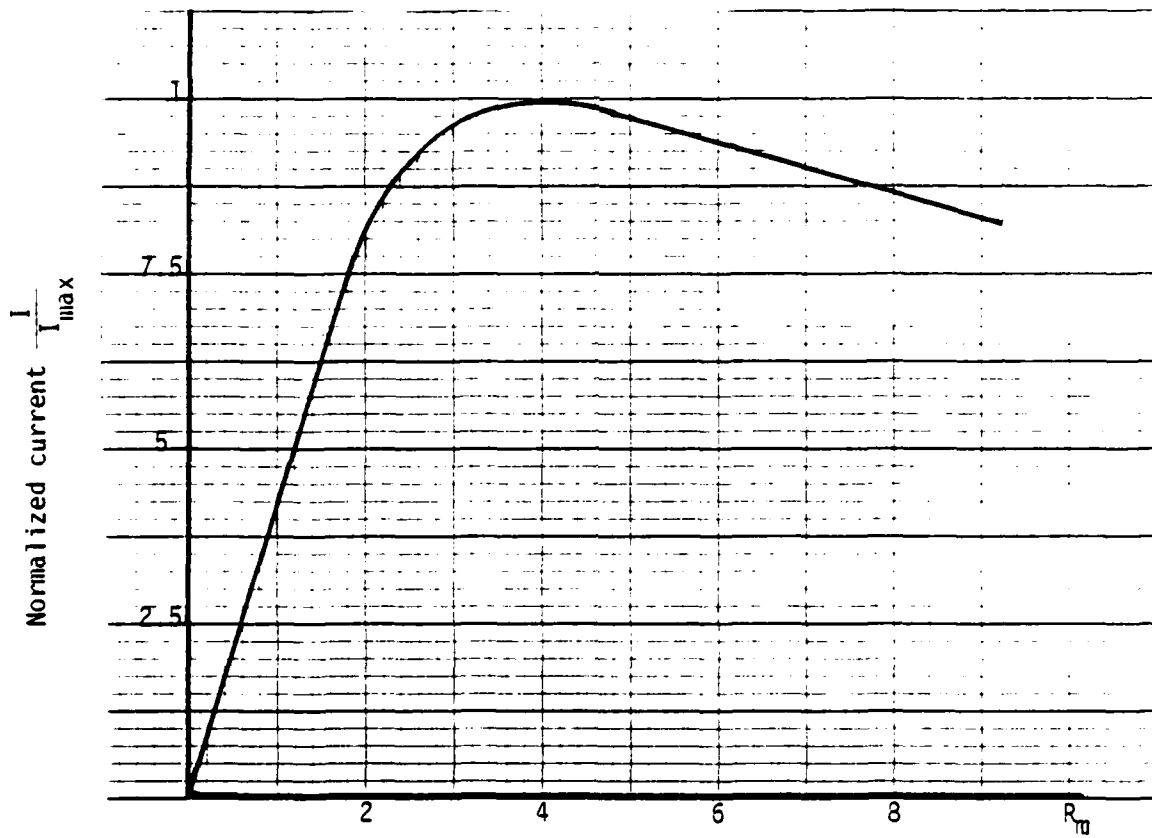


Figure 20 - Dependence Of The Normalized Maximum Current Generated By The Pump As A Function Of The Speed Of Rotation (or Reynolds number R_m).

SECTION IX
SCALING LAWS FOR FLUX PUMPS

In spite of the complicated theory for the distribution of current in the superconducting sheet, some simple laws can be obtained for the performance of the pump.

On the basis of Eq. (5), the pumping rate is given by

$$\frac{dI}{dt} = \left(\frac{Nf\phi}{L} \right) \quad (24)$$

As explained in a previous section, provided one operates the pump in a regime of low Reynolds number, the pumping rate increases linearly with the number of poles, the field strength in the gap, and the speed of rotation. It is of advantage, therefore, to use higher fields and materials with higher quenching fields, larger pole faces and higher speeds.

To take into account the diffusion in the magnetic field, a careful calculation of the current in the interface of the normal/superconducting region was performed (Ref. 8). A correction to Eq. (24) is needed so that the dependence of the pumping on the speed is expressed by a new relation of the form

$$\frac{I}{I_{\max}} = \frac{N\phi f}{L} F(R_m)$$

where $F(R_m)$ shown in graphical form in Fig. 20 was calculated numerically in Ref. (8).

SECTION X CONCLUSION

The series of tests described in the measurements section showed in a convincing manner that the concept of a brushless generator as described in this report is feasible. The ability of "charging" the superconducting coils and maintaining a circulating current in them is also demonstrated. It was also shown that the flux pump could discharge the coils at a rate equal to the pumping rate.

The flux pump that was built turned out to have a number of drawbacks. All of these, however, can be remedied quite readily by modifying the design. The generator was meant to be rotated at 500 rpm. Misalignment, because of the inordinate length of the generator, forced us to restrict the work to lower speed and, hence, to lower flux pumping rates. Present state-of-the-art in a generator, would not use a dewar but would instead rely on a rotating manifold to allow for the continuous flow of liquid helium. As a result, the machine is shorter and the generator can be made to rotate easily 20 to 50 times faster. At these speeds, it is quite feasible for the current to reach its maximum value of 1000 amps in a fraction of a second, more accurately between $\frac{1}{100}$ to $\frac{1}{1000}$ of a second for a six pole machine with an RPM of 10,000.

When forced cooling is used, it is visualized that the flux pump can carry larger currents without any difficulty. Maximum currents between 50 to 100 thousand amps are attainable. As a matter of fact, these large currents were already obtained in the slower and cruder machines constructed by Volger and Wipf and which we referred to in the report.

The efficiency of the flux pump, in spite of all these failings, turned out to be remarkably high. It was pointed out in the report that simple corrective measures, in the shape of the field and the size of the pump can raise the efficiency from the 93% that was found, to a realistic figure of 99% or better.

Finally, the thermal losses in the slip rings encountered in conventional machines are completely eliminated in the brushless generator. This is a very important advantage in that it yields a great savings in weight of the helium cooling power plant.

REFERENCES

1. O.K. Mawardi et al., IEEE Trans. on Magnetics MAG-13, 780, (1976).
2. The list given below is representative of the major work done in the development of flux pumps: H. Van Beelen et al., Phys. Letters 4, 310 (1963) and 1, 175 (1963); J.F. Marchand and J. Volger, Phys. Letters 2, 118 (1962); Marchand, J.F. and Volger, J., Physics Lett. 2, 118 (1962); Mendelssohn, K., Nature 132, 602 (1933); Swarg, P.S. and Rosner, C.H., J. Appl. Phys. 33 2292 (1962); Hildebrandt, A.F. et al., J. Appl. Phys. 33, 2375 (1962); Felici, N.J. C.R. Acad. Sci., Paris 20b, 242, 599 (1938); Olsen, J.L., Rev. Sci. Instr. 29, 537 (1958); Laquer, H.L., Cryogenics 3, 27 (1963); Buchheld, T., Cryogenics 4 212 (1964); Felici, N.J., Am. Phys. Paris 13, 266 (1940); D. van Houwelingen, Admiraal P.S., and J. van Suchtelen, J. Phys. Lett. 8, 310 (1964).
3. J. Volger, Advances in Cryogenic Engineering, Vol. (10), 98 (Plenum Press, New York 1965).
4. J. Volger et al., Philips Tech. Rev. 24, 399 (1963).
5. S.L. Wipf, Advances in Cryogenic Engineering Vol. (9), 342 (Plenum Press, New York (1964).
6. T. Cowling "Magnetohydrodynamics" (Interscience New York, 1957).
7. Ref. (3).
8. O.K. Mawardi et al., IEEE Trans. on Magnetics MAG-15, 828 (1979).
9. O.K. Mawardi et al., Electric Power Research Inst. (EPRI EL-479), 1978.

BIBLIOGRAPHY

The following references are of general interest to the study of flux pumps and provide additional background material.

D. Shoenberg, "Superconductivity", Cambridge University Press, 1965.

C.G. Kuper, "An Introduction to the Theory of Superconductivity", Clarendon Press, Oxford, 1968.

F. London, "Superfluids", Vol. I, Dover Publications, N.Y., 1961.

A.C. Rose-Innes, "A Superconducting Magnetic Flux Compressor", Cryogenics, Vol. 13, p. 103, 1973.

A.F. Hildebrandt et al., "Some Experimental Consequences of Flux Conservation within Multiply-Connected Superconductors", J. of Appl. Phys., Vol. 33, No. 7, 1962.

N.J. Felici, C.R. Ac d. Sci., Paris, Vol. 206, p. 242, 1938, from ref. (8).

D. Van Houwelingen and J. Volger, "The Superconducting Dynamo Properties and Applications", Philips Research Reports, Vol. 23, No. 3, p. 249, 1968.

J. Van Suchtelen et al., "The Principle and Performance of a Superconducting Dynamo", Cryogenics, Vol. 5, p. 256, 1965.

H. Van Beelen et al., "Flux Pumps and Superconducting Solenoids", Physica, Vol. 31, p. 413, 1965.

M.S. Lubell and S.L. Wipf, "A Cabled-Wire Magnet Powered by a Flux Pump", Advances in Cryogenic Engineering, Vol. 13, p. 150, 1968.

S.L. Wipf, "A Superconducting Direct-Current Generator", Advances in Cryogenic Engineering, Vol. 9, p. 342, 1964.

S.L. Wipf, "The Case for Flux Pumps and Some of Their Problems", Proc. 1968 Summer Study on Supercond. Devices and Accel., Brookhaven Nat'l Lab., p. 632, 1968.

A.R. Sass, "Analysis of a Distributed Superconductive Energy Converter", IEEE Trans. on Aerospace, Vol. 2, No. 2, p. 822, 1964.

S.L. Wipf, "Flux Pumps as Power Supplies for Superconducting Coils", Proc. Int'l Symp. on Magnet Technology, Stanford, p. 615, 1965.

A.B. Pippard, "Kinetics of the Phase Transition in Superconductors", Phil. Mag., Vol. 41, No. 3, p. 243, 1950.

I.M. Lifshitz, "The Kinetics of the Breakdown of Superconductivity by a Magnetic Field", Zhur, Eksptl. i Teoret. Fiz., Vol. 20, No. 9, p. 834, 1950.

I.M. Lifshitz, "The Kinetics of the Breakdown of Superconductivity by an Alternating Field", Doklady Adad. Nauk SSSR, Vol. 90, No. 3, p. 363, 1953.

BIBLIOGRAPHY, CON'T

C.J. Gorter, "On the Possibility of a Dynamic Variety of the Intermediate Superconductive State", *Physica*, Vol. 23, p. 45, 1957.

C.J. Gorter and M.L. Potters, "On the Motion of the Boundary Between the Normal and Superconductive State in Cylindrical Wire Carrying a Strong Current", *Physica*, Vol. 24, p. 169, 1958.

F. Rothen and W. Bestgen, "Kinetics of the Destruction of Type I Superconductivity by a Current", *Physik Der Kondensierten Materie*, Vol. 12, p. 311, 1971.

O.K. Mawardi, "Operational Characteristics of Rotating Flux Pumps", CWRU Internal Report, 1976.

O.K. Mawardi et al., "Brushless Superconducting Alternators", *IEEE Trans. on Magnetics*, Vol. MAG-13, No. 1, 1977.

R.S. Thompson and C.R. Hu, "Dynamic Structure of Vortices in Superconductors", *Phys. Rev. Letters*, Vol. 27, No. 20, p. 1352, 1971.

C.R. Hu and R.S. Thompson, "Dynamic Structure of Vortices in Superconductors. II. $H \ll H_{c2}$ ", *Phys. Rev. B*, Vol. 6, No. 1, p. 110, 1972.

R.S. Thompson et al., "Dynamic Structure of Vortices in Superconductors. III. Graphs for $B \approx H_{c2}$ ", *Phys. Rev. B*, Vol. 6, No. 5, p. 2044, 1972

H.K. Chung, "A Superconducting SKRAM Generator", Master Thesis CWRU, 1977.

A.F. Andreev, "Electrodynamics of the Intermediate State", *Soviet Physics JETP*, Vol. 24, No. 5, 1967.

I.N. Sneddon, "Elements of Partial Differential Equations", McGraw-Hill, N.Y., 1957.

E.G. Brentari and R.V. Smith, "Nucleate and Film Pool Boiling Design Correlations for O₂, N₂, H₂ and He", *Int'l. Advances in Cryogenics Engineering*, p. 325, 1965.

D.N. Lyon, "Boiling Heat Transfer and Peak Nucleate Boiling Fluxes in Saturated Liquid Helium Between the λ and Critical Temperatures", *Int'l. Advances in Cryogenic Engineering*, p. 371, 1965.

S.G. Sydoriak, "Cryostatic Stability Equation", *IEEE Trans. on Magnetics*, Vol. MAG-13, No. 1, p. 682, 1977.

E.R. Andrew and J.M. Lock, "The Magnetization of Superconducting Plates in Transverse Magnetic Fields", *Proc. Phys. Soc. (London)*, Vol. A63, p. 13, 1950.

R.B. Ross, "Metallic Materials", Chapman & Hall, London, 1968.

B.W. Roberts, "Superconductive Materials", *J. Phys. Chem. Ref. Data*, Vol. 5, No. 3, 1976

BIBLIOGRAPHY, CON'T

G.W. Webb, "Low Temperature Electrical Resistivity of Pure Niobium", Phys. Rev., Vol. 181, No. 3, 1969.

J. Kirschenbaum, "Superconducting Critical Fields in Niobium and Niobium Containing Oxygen" Phys. Rev. B, Vol. 12, No. 9, 1975.

P.H. Kes et al., "Thermal Conductivity of Niobium in the Purely Superconducting and Normal States", J. Low Temp. Phys., Vol. 17, No. 314, p. 341, 1974.

Y. Muto et al., "Thermal Conductivity of Pure Niobium in the Superconducting, Mixed and Normal States", Proc. 11th Int'l. Conf. on Low Temp. Phys., St. Andrews, 1968, p. 930.

J.F. DaSilva et al., "Low Temperature Specific Heat of Annealed High Purity Niobium in Magnetic Fields", Physica, Vol. 41, p. 409, 1969.

XI

PRELIMINARY HAZARD ANALYSIS

System Description

The system consists of a vacuum system, a mechanical drive and of the brushless superconducting generator. The vacuum system is needed to maintain a vacuum around the generator for the purpose of minimizing the thermal losses. The drive is extraneous to the system and consists of a prime mover needed to rotate the shaft of the generator. The brushless superconducting generator is maintained at liquid helium temperature. Electric power is generated as a result of the relative motion of conductors in the magnetic field produced by superconducting field coils.

Hazard Analysis

The brushless superconducting generator described in this report is a new experimental machine which has never been built before. Our experience with such a device is as far as the system reliability safety and hazard, therefore is non-existent.

A further comment is that the actual construction of the device for field use will be drastically different from the experimental version described in this report. The speculation of the hazards of a non-existent design becomes pointless.

DATE
LME
-8